

Quantifying biases in TROPESS AIRS, CrIS, and joint AIRS+OMI tropospheric ozone products using ozonesondes

Elyse A. Pennington¹, Gregory B. Osterman¹, Vivienne H. Payne¹, Kazuyuki Miyazaki¹, Kevin W. Bowman¹, and Jessica L. Neu¹

¹Jet Propulsion Laboratory, California Institute of Technology

Correspondence: Elyse A. Pennington (elyse.a.pennington@jpl.nasa.gov)

Abstract. Quantifying changes in global and regional tropospheric ozone are critical for understanding global atmospheric chemistry and its impact on air quality and climate. Satellites now provide multi-decadal records of daily global ozone profiles, but previous studies have found large disagreements in satellite-based ozone trends, including in trends from different products based on the same spectral radiances. In light of these disagreements, it is critical to quantify to what degree the observed trend is attributable to measurement error for each product by comparing satellite-retrieved ozone to long-term measurements from ozonesondes. NASA's TROPESS project provides satellite retrievals of ozone from a suite of instruments, including CrIS, AIRS, and multispectral combinations such as AIRS and OMI (joint AIRS+OMI) using a common algorithm. We compare these products to ozonesondes and find that the evolution of global tropospheric ozone satellite-sonde bias for TROPESS CrIS ($0.21 \pm 3.6\%$ decade⁻¹, 2016-2021), AIRS ($-0.41 \pm 0.57\%$ decade⁻¹, 2002-2022), and joint AIRS+OMI ($1.1 \pm 1.0\%$ decade⁻¹, 2004-2022) are less than the magnitude of trends in global tropospheric ozone reported by the Tropospheric Ozone Assessment Report Phase 1 (TOAR-I). We further quantify the bias in regional trends, which tend to be higher but with a smaller number of sondes, which can impact the satellite-sonde bias and trend. Our work represents an important basis for the utility of using satellite data to quantify changes in atmospheric composition in future studies.

Copyright statement. © 2025. California Institute of Technology. Government sponsorship acknowledged.

1 Introduction

Tropospheric ozone trends show large regional variations and can depend strongly on the type of measurement analyzed, coverage, frequency, and vertical sensitivity. The Tropospheric Ozone Assessment Report (TOAR, <https://igacproject.org/activities/TOAR>) aims to provide the most complete assessment of tropospheric ozone available to the community by compiling a comprehensive database of ozone measurements and analyzing data from multiple sources holistically. The Sixth Assessment Report (AR6) produced by the Intergovernmental Panel on Climate Change (IPCC) reports that the global tropospheric ozone burden (TOB) is increasing, but regional trends detected by three ensembles of satellite data ranged in magnitude from 2% decade⁻¹ to 14%

decade⁻¹ (Gulev et al., 2021). The ensembles in Gulev et al. (2021) combine satellite instruments that retrieve ozone in the ultraviolet (UV), visible, and/or near infrared (NIR) ranges, but do not include instruments that retrieve ozone in the thermal infrared (TIR) range. Some TIR instruments have reported negative tropospheric ozone trends in various regions (e.g., Pope et al., 2024; Dufour et al., 2025). The satellite assessment in Phase 1 of TOAR (TOAR-I; Gaudel et al., 2018) speculated that causes of inter-satellite disagreement include differences in each instrument’s vertical sensitivity to the atmospheric profile of ozone, spatial sampling across the globe, and measurement period.

Ongoing work in TOAR Phase 2 (TOAR-II) aims to investigate the causes of measurement-dependent differences in ozone trends and find consensus across techniques to determine the true TOB trend. There are a range of reported tropospheric ozone trends from work published in the past decade (Table 1), which tend to agree that tropospheric ozone is increasing globally and in most specific latitude bands, but to varying degrees and with varying levels of certainty. These recent works discuss two major reasons for discrepancies between satellite ozone products. The first is that the vertical sensitivity of each instrument impacts the amount of measured ozone in each level of the atmosphere (Gaudel et al., 2018). Some instruments and retrievals can distinguish influences from the upper versus lower troposphere (Pope et al., 2023, 2024; Froidevaux et al., 2024), which can lead to different assessments of how tropospheric ozone is changing if these changes are not uniform in altitude. Second, the satellite product quality can drift over time, producing an artificial trend caused by error in the instrument calibration or retrieval (Gaudel et al., 2018). Gaudel et al. (2024) demonstrated a method to correct the tropospheric ozone trend for the time-dependent bias, to produce a "true" tropospheric ozone trend. This was accomplished by quantifying the bias between satellite data and a reference method, for example ozonesonde data. The magnitude of bias was used to scale the satellite data to determine trends in tropospheric ozone with the retrieval bias (approximately) removed.

Table 1: Tropospheric ozone burden (TOB) trends from satellite products reported in the literature. LT = lower troposphere. UT = upper troposphere. For the RAL merges product, uncertainty is displayed at the 95% confidence interval.

| Product / Measurement | Trend (±Uncertainty) | Region | Date Range | Reference |
|-----------------------|-------------------------------------|-------------|------------|--------------------------|
| Harmonized CCD | 0.7 (±1.2) DU decade ⁻¹ | tropics | 1995-2015 | Heue et al. (2016) |
| Harmonized CCD | -0.2 (±0.6) DU decade ⁻¹ | tropics | 1996-2015 | Leventidou et al. (2018) |
| OMI/MLS | 1.79 (±0.66) Tg yr ⁻¹ | 60°S - 60°N | 2005-2016 | Gaudel et al. (2018) |
| IASI-FORLI | -2.15 (±1.03) Tg yr ⁻¹ | 60°S - 60°N | 2008-2016 | Gaudel et al. (2018) |
| IASI-SOFRID | -1.34 (±0.92) Tg yr ⁻¹ | 60°S - 60°N | 2008-2015 | Gaudel et al. (2018) |
| GOME/OMI | 1.63 (±0.45) Tg yr ⁻¹ | 60°S - 60°N | 1996-2015 | Gaudel et al. (2018) |
| OMI-RAL | 2.85 (±1.16) Tg yr ⁻¹ | 60°S - 60°N | 2005-2015 | Gaudel et al. (2018) |
| SCIAMACHY | 1.50 (±1.39) Tg yr ⁻¹ | 60°S - 60°N | 2002-2012 | Gaudel et al. (2018) |
| OMI/MLS | 1-3 DU decade ⁻¹ | 90°S - 90°N | 2005-2016 | Ziemke et al. (2019) |
| Merged TOMS, OMI/MLS | ≈3.1 ppbv decade ⁻¹ | 0°- 30°N | 1979-2016 | Gulev et al. (2021) |

| | | | | |
|--|---|-------------|-----------|--------------------------|
| Merged TOMS, OMI/MLS | ≈ 1.7 ppbv decade ⁻¹ | 30°S - 0° | 1979-2016 | Gulev et al. (2021) |
| Merged GOME, SCIAMACHY, OMI, GOME-2A, GOME-2B | ≈ 1.0 ppbv decade ⁻¹ | 20°S - 20°N | 1995-2015 | Gulev et al. (2021) |
| Merged GOME, SCIAMACHY, GOME-II | ≈ -0.2 ppbv decade ⁻¹ | 15°S - 15°N | 1995-2015 | Gulev et al. (2021) |
| OMI/MLS | 1.4 ppb decade ⁻¹ | 90°S - 90°N | 2005-2019 | Fadnavis et al. (2024) |
| OMI/MLS | 0.96 (± 0.45) DU decade ⁻¹ | 60°S - 60°N | 2005-2019 | Elshorbany et al. (2024) |
| OMI/MLS | 1.06 (± 0.40) DU decade ⁻¹ | 30°S - 30°N | 2005-2019 | Elshorbany et al. (2024) |
| OMI/MLS | 0.78 (± 1.16) DU decade ⁻¹ | 30°N - 60°N | 2005-2019 | Elshorbany et al. (2024) |
| OMI/MLS | 0.95 (± 0.75) DU decade ⁻¹ | 30°S - 60°S | 2005-2019 | Elshorbany et al. (2024) |
| OMI/MLS | 1.6 (± 1.1) Tg decade ⁻¹ | 0° - 20°N | 2004-2019 | Gaudel et al. (2024) |
| OMI | 2.4 (± 1.1) Tg decade ⁻¹ | 0° - 20°N | 2004-2019 | Gaudel et al. (2024) |
| OMI/MLS | 0.9 (± 2.2) Tg decade ⁻¹ | 0° - 20°S | 2004-2019 | Gaudel et al. (2024) |
| OMI | 1.9 (± 2.4) Tg decade ⁻¹ | 0° - 20°S | 2004-2019 | Gaudel et al. (2024) |
| RAL merged product (LT) | 4.49 (2.51, 6.48) DU decade ⁻¹ | 60°S - 45°S | 1996-2017 | Pope et al. (2023) |
| RAL merged product (LT) | 1.85 (0.11, 3.59) DU decade ⁻¹ | 45°S - 30°S | 1996-2017 | Pope et al. (2023) |
| RAL merged product (LT) | 0.94 (-1.05, 2.93) DU decade ⁻¹ | 30°S - 15°S | 1996-2017 | Pope et al. (2023) |
| RAL merged product (LT) | 2.89 (1.27, 4.52) DU decade ⁻¹ | 15°S - 0° | 1996-2017 | Pope et al. (2023) |
| RAL merged product (LT) | 3.93 (3.13, 4.72) DU decade ⁻¹ | 0° - 15°N | 1996-2017 | Pope et al. (2023) |
| RAL merged product (LT) | 4.12 (3.25, 4.97) DU decade ⁻¹ | 15°N - 30°N | 1996-2017 | Pope et al. (2023) |
| RAL merged product (LT) | 1.33 (-0.34, 3.01) DU decade ⁻¹ | 30°N - 45°N | 1996-2017 | Pope et al. (2023) |
| RAL merged product (LT) | 0.49 (-1.14, 2.13) DU decade ⁻¹ | 45°N - 60°N | 1996-2017 | Pope et al. (2023) |
| MLS (UT) | 0.22 (± 0.16) ppbv yr ⁻¹ | 20°S - 20°N | 2005-2020 | Froidevaux et al. (2024) |

Ozonesondes provide a long-term record of detailed vertical ozone profiles and thus are an important tool for quantifying the vertical distribution of ozone and therefore have been useful in validating satellite retrievals of ozone. Ozonesondes are mounted on atmospheric balloons that are routinely launched from over 40 sites worldwide (WMO/GAW, 2024). These sites are distributed unevenly, with many sites located in North America and Europe, and fewer sites in the Southern Hemisphere. There are multiple types of ozonesondes, including electrochemical concentration cells (ECC; Komhyr, 1969; Komhyr and Harris, 1971; Tarasick et al., 2021; WMO, 2021) and Brewer-Mast (BM; Brewer et al., 1997; Steinbrecht et al., 1998) sondes. Most ozonesonde launch sites use ECC sondes, which typically have an uncertainty of 10-20% (WMO, 2021). The Harmonization and Evaluation of Ground-based Instruments for Free Tropospheric Ozone Measurements (HEGIFTOM) Working Group of TOAR-II was developed with the goal of improving the accuracy and precision of ozone measurements by remov-

ing inhomogeneities between ozonesondes caused by differences in equipment, operating procedures, or data processing. The Working Group utilized a harmonization technique to address this need and have reduced ozonesonde measurement uncertainty to 5% (5-10% in the tropics) (WMO, 2021). The state-of-the-art method produces sonde data with high accuracy, precision, and long-term reliability, making them a good tool for validating other measurement methods.

We introduce here three satellite tropospheric ozone products that were not part of the TOAR-1 assessment and use the HEGIFTOM ozonesonde measurements to assess their suitability for quantifying trends in TOB. The Tropospheric Ozone and its Precursors from Earth System Sounding (TROPESS) project (NASA, 2024) provides retrievals of ozone and other trace gases from a suite of satellite instruments, including the Cross-track Infrared Sounder (CrIS), Atmospheric Infrared Sounder (AIRS), and a joint retrieval product using AIRS and the Ozone Monitoring Instrument (OMI) (joint AIRS+OMI). These satellite products provide long-term records of ozone using a consistent retrieval algorithm that produces ozone profiles that use the same *a priori* profiles and are calculated on the same vertical grid and with the same method of uncertainty estimation, making them more readily comparable. This study aims to validate the accuracy of TROPESS satellite retrievals of tropospheric ozone and their stability with time against ozonesonde measurements. Section 2 introduces the satellite and ozonesonde datasets and describes the analysis tools used to compare them. Section 3 presents comparisons between satellite and ozonesonde profiles and columns, long-term trends in the satellite-sonde bias, and temporal and geographic variations in these quantities.

2 Data and methods

2.1 TROPESS ozone retrievals

All TROPESS Level 2 data is produced using the MUSES — MUlti-SpEctra, MUlti-SpECies, MUlti-SEnsors — algorithm (Fu et al., 2013, 2016, 2018) following the optimal estimation methods employed for the EOS Tropospheric Emission Spectrometer (TES) (Beer, 2006; Bowman et al., 2006). This approach estimates vertical profiles, uncertainty estimates, and observation operators, which are critical for chemical data assimilation and inverse modeling (Jones et al., 2003; Parrington et al., 2009; Miyazaki et al., 2017, 2020b). Three TROPESS products are considered in this study, CrIS, AIRS, and the joint AIRS+OMI retrieval, and have been used in previous studies to, for example, monitor changes in global tropospheric ozone (Miyazaki et al., 2021) and understand the processes controlling air pollution (Miyazaki et al., 2019).

CrIS, AIRS, and OMI data have been used to generate Level 2 products by other teams and retrieval algorithms. For example, the Community Long-term Infrared Microwave Combined Atmospheric Product System (CLIMPCAPS), NOAA Unique Combined Atmospheric Processing System (NUCAPS), and Near Real Time (NRT) Standard Physical Retrieval (AIRS2RET_NRT_7.0) produce Level 2 CrIS and AIRS products that are retrieved from Level 2 cloud cleared radiances on a 45 km field of regard (Smith and Barnett, 2020; Barnett et al., 2021; AIRS, 2019). The single field-of-view (SFOV) sounder atmospheric product (SiFSAP) retrieval algorithm produces Level 2 CrIS, AIRS, and IASI products from Level 1B radiances (Wu et al., 2023). The TROPESS project generates Level 2 products using Level 1B radiances processed by the MUSES algorithm. The three TROPESS products are described further in Sect. 2.1.1-2.1.3.

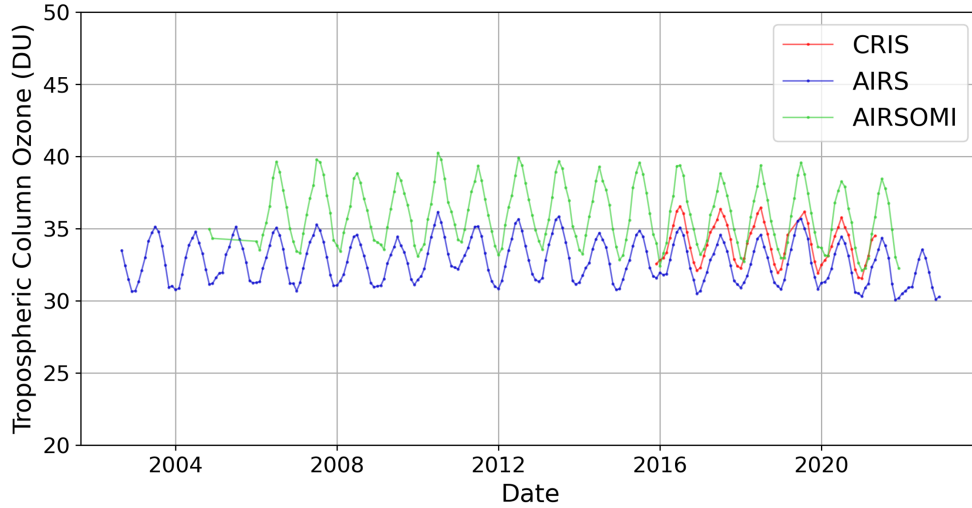


Figure 1. Global (67°S-85°N) monthly average tropospheric ozone columns for the TROPESS CrIS (red), AIRS (blue), and joint AIRS+OMI (green) products.

The global, monthly average tropospheric ozone columns are computed from the ozone profiles retrieved by MUSES and are shown in Fig. 1 for the three products. The average tropospheric column — integrated over the ozone profile from the surface to the thermal tropopause (see Sect. 2.3) — falls between 30 and 40 Dobson Units (DU), with the ozone seasonal cycle clearly visible. Each satellite product provides data for different time periods and with different average magnitudes, which will be discussed in Sect. 3. The trends in the TROPESS ozone products are not monotonic largely due to the decrease in ozone during the COVID-19 pandemic (Miyazaki et al., 2021). Therefore, they require careful consideration when being compared to the trends in bias shown in the current study. Such analysis will be the topic of a follow-on manuscript.

2.1.1 CrIS

CrIS is on the Suomi National Polar-orbiting Partnership (SNPP) satellite, which was launched on October 28, 2011 and has a 13:30 local time ascending node (Han et al., 2013). CrIS instruments are also flying on the Joint Polar Satellite Series platforms (JPSS-1 and JPSS-2). However, for this study we focus only on SNPP-CrIS data so that we use one consistent record (with, e.g., consistent calibration, spatial sampling, and temporal sampling) for our trend analysis. CrIS has high spectral resolution, high signal-to-noise ratio, and a low calibration uncertainty (Han et al., 2013; Strow et al., 2013; Tobin et al., 2013; Wang et al., 2013). CrIS measures infrared (IR) radiances in 3 bands: 650-1090 cm^{-1} (long-wave IR, LWIR), 1210-1750 cm^{-1} (mid-wave IR, MWIR), and 2155-2550 cm^{-1} (short-wave IR, SWIR) (Han et al., 2013). TROPESS ozone retrievals from CrIS specifically use 4 windows in the LWIR and 6 windows in the MWIR (Malina et al., 2024). TROPESS CrIS Level 2 products are retrieved from the L1B radiances on individual 15 km fields of view. The CrIS data record begins in 2012 but the radiance data that was initially retrieved only has nominal spectral resolution (NSR): 0.625 cm^{-1} in the LWIR band, 1.25 cm^{-1} in the

MWIR band, and 2.5 cm^{-1} in the SWIR band (Han, 2015). In November 2015, the data record grew to include the full spectral resolution (FSR) of 0.625 cm^{-1} in all three bands. The TROPES project uses the NASA L1B FSR radiance data (Revercomb and Strow, 2018) so our record begins in November 2015 (Han, 2015). In late March 2019, there was an anomaly in the MWIR band, resulting in a gap in data from April through July 2019. The instrument was restored to full functionality, and there is good consistency between the early and later 2019 data (Iturbide-Sanchez et al., 2022). In July 2021, there was a failure in the LWIR bands that required the instrument to change to a different set of electronics (NOAA, 2021), and the data acquired after this date was no longer included in the long-term record by NASA. Therefore, the ozone record used in this study runs from December 2015 through May 2021. Given the large variability in tropospheric ozone and the small magnitude of its trends, the TROPES CrIS record is too short to detect ozone trends with good statistical significance. Nonetheless, we consider the time dependence of the CrIS-sonde bias using the same analysis process as with the other two TROPES products because we focus here on whether there are any changes in the retrieval quality with time as well as on the consistency of the TROPES products. In particular, TROPES CrIS and AIRS both utilize IR radiances, and their comparison is of particular interest. We discuss the impact of the relatively short CrIS time range with respect to bias detection in Sect. 3.2. Our analysis is a necessary step if the TROPES CrIS product is to be used as part of a longer-term merged tropospheric ozone record in the future.

2.1.2 AIRS

AIRS is a thermal infrared (TIR) grating spectrometer onboard the Aqua satellite, launched on May 4, 2002 (Aumann et al., 2003; Susskind et al., 2003, 2014). Aqua is part of the A-train, a constellation of satellites that orbit together (Stephens et al., 2002). AIRS has a 13 km footprint at nadir and measures in the $650\text{--}2675\text{ cm}^{-1}$ wavelength range (Aumann et al., 2003; Susskind et al., 2003), with ozone retrieved from channels around 1042 cm^{-1} (Wei et al., 2010). Similarly to CrIS, TROPES retrieves ozone from AIRS from L1B radiances (AIRS, 2007) using 10 distinct wavelength windows in the IR (Fu et al., 2018). TROPES AIRS Level 2 products are retrieved from the L1B radiances on individual 15 km fields of view.

2.1.3 Joint AIRS+OMI retrieval

OMI, unlike CrIS and AIRS, measures ozone-absorbing radiances in the UV range (Levelt et al., 2006, 2018; Liu et al., 2010b, a; Huang et al., 2017). OMI flies on the Aura satellite, a member of the A-train, so it collects data at nearly the same local time as AIRS. Retrievals of ozone from OMI use wavelengths between 270 and 365 nm with a ground pixel size of $12 \times 24\text{ km}$ (Levelt et al., 2006). OMI experienced a "row anomaly" beginning in 2007. In 2009, the anomaly spread and many pixels became unusable; since 2010, ~40-50% of OMI pixels must be discarded. In addition to the lower data volume, there have been small changes to OMI radiances (1-2%) and irradiances (3-8%), but overall the number of good pixels remains stable (Schenkeveld et al., 2017).

Fu et al. (2018) combined AIRS and OMI radiances in a joint retrieval to produce the joint AIRS+OMI product. This multispectral retrieval, implemented in the MUSES algorithm, uses information in the AIRS TIR bands and the OMI UV bands to produce vertical ozone profiles. The joint AIRS+OMI product has greater vertical sensitivity than the AIRS or OMI retrievals alone, with degrees of freedom of signal (DOFS) in the troposphere ranging from 0.2 to 1.6, typically falling above

135 1 (Fu et al., 2018). Because the DOFS exceeds 1, it is possible to resolve ozone subcolumns in the troposphere, i.e., upper and lower tropospheric ozone.

2.2 Ozonesonde data

ECC sondes are mounted alongside radiosondes to provide the partial pressure of ozone, total atmospheric pressure, and atmospheric temperature (Tarasick et al., 2019). These quantities can be used to calculate the volume mixing ratio (VMR) of ozone throughout the profile until the balloon pops, typically before reaching 5 hPa. Ozonesonde data is provided by the HEGIFTOM Working Group of TOAR-II (Van Malderen et al., 2025). The sonde launch sites providing data for this study are shown in Fig. 2a.

2.2.1 Coincidence criteria

Sonde and satellite profiles are compared if the sonde is launched within 300 km and 9 hours of the satellite measurement. These criteria may result in multiple satellite profiles being matched with a single sonde profile. These spatial and temporal thresholds were chosen to compare measurements from similar air masses while being large enough to capture sufficient data for a statistically meaningful comparison, and to maintain consistency with previous studies (Nassar et al., 2008; Verstraeten et al., 2013). However, the choice of coincidence criteria can impact the satellite-sonde bias. Nassar et al. (2008) showed that wide spatial and temporal coincidence criteria can lead to comparisons between satellite and sonde profiles that measured air columns with high atmospheric and ozone variability. When they tightened the spatial and temporal coincidence criteria, the value of the bias did not change in a statistically meaningful way, but the standard deviation increased. This implies that comparing profiles with different atmospheric profiles adds random error but does not introduce a positive or negative bias (Nassar et al., 2008). So, we maintain these coincidence criteria — 300 km and 9 hours — in our study.

2.2.2 Application of the satellite operator

To directly compare satellite and sonde profiles, the satellite retrieval operator must be applied to the sonde data to account for satellite sensitivity and vertical resolution (Jones et al., 2003; Worden et al., 2007; Verstraeten et al., 2013; Malina et al., 2024). This operation is performed on the sonde data to estimate the ozone profile that the satellite would have measured had it observed the same air mass as the sonde, with no systematic or random errors other than those attributable to the smoothing of the profile due to the vertical sensitivity of the satellite. The satellite operator includes the averaging kernel and *a priori* constraint vector together; examples of these quantities are shown in Fig. 3. The following steps describe the application of the satellite operator to a sonde profile.

1. Sonde measurements are provided on fine vertical grids with variable maximum altitudes. All TROPES profiles are provided on 67 fixed levels reaching a minimum pressure of approximately 1 hPa. For a matched pair of a satellite profile and sonde profile, if the minimum pressure (i.e., maximum altitude) of the sonde profile is greater than the minimum pressure of the satellite profile, then the ozone concentrations from the satellite prior are appended to the sonde profile

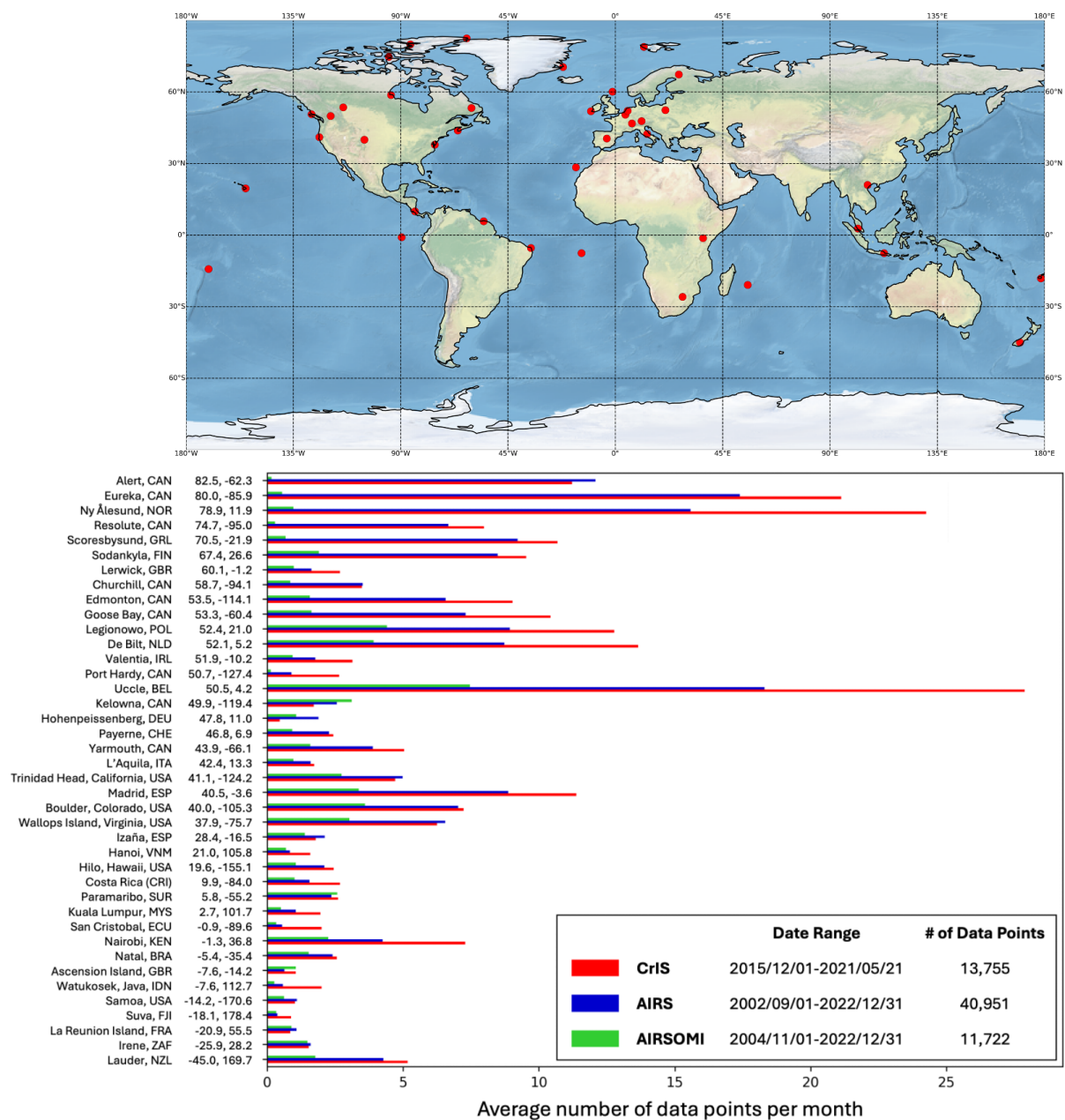


Figure 2. (a) Ozonesonde launch sites providing harmonized data in this study. (b) Monthly average number of matched satellite-sonde data points at each sonde launch site for each satellite product. Sites are ordered by decreasing latitude. The figure legend provides the date range of each satellite product and the total number of matched satellite-sonde data points over the date range at all sites.

concentrations, scaling the prior so that the concatenated concentration profile is continuous. This step ensures that the satellite and sonde profiles reach the same minimum pressure.

2. The sonde profile is interpolated to the same 67 pressure levels as the satellite profile.

3. The satellite operator is applied according to Equation 1. \mathbf{x}_{sonde} is the new sonde profile, which can be directly compared
170 to the satellite profile, \mathbf{x}_a is the *a priori* profile, \mathbf{A} is the averaging kernel, and $\mathbf{x}_{sonde,measured}$ is the sonde profile
produced following steps 1 and 2. Example profiles and averaging kernel from a single CrIS sounding are presented in
Fig. 3, and representative averaging kernels for each instrument are given in Fig. S4.

$$\mathbf{x}_{sonde} = \mathbf{x}_a + \mathbf{A}(\mathbf{x}_{sonde,measured} - \mathbf{x}_a) \quad (1)$$

After the satellite operator is applied to the sonde profile, the profiles must be quality controlled. Poor quality in the resampled
175 sonde profiles may result from either poor quality in the original sonde profiles ($\mathbf{x}_{sonde,measured}$) or poor behavior when the
satellite operator is applied to $\mathbf{x}_{sonde,measured}$. The HEGIFTOM group did not quality control (QC) the sonde data, so we
tested multiple methods of QC, explained in Sect. S1. To evaluate each QC method, we considered the impact on the mean,
median, standard deviation, and trend of the tropospheric ozone column satellite-sonde bias, as well as the percentage of
profiles removed. See Sect. S1 for a detailed description of the methods that were tested and the metrics used to evaluate the
180 QC methods.

Our selected quality control method considers the stratosphere and troposphere separately. In the stratosphere, profiles are
compared to a climatology from the Aura Microwave Limb Sounder (MLS), an instrument launched in 2004 onboard the
Aura satellite that provides stratospheric profiles of multiple atmospheric gases (Livesey et al., 2022; Waters et al., 2006;
Werner et al., 2023) and has been validated using ozonesonde and lidar measurements (Jiang et al., 2007). The accuracy of
185 the MLS-retrieved ozone in the upper troposphere is within 5% compared to ozonesonde data, except in the tropics where the
 2σ uncertainty can reach 10% (Livesey et al., 2022). The Level 3 MLS dataset includes the mean ozone profile and standard
deviation at each level, binned into latitude bands spaced every 10° (Fig. S5). We assume that any ozone mixing ratio that falls
outside of the mean MLS profile ± 5 standard deviations in a specific latitude band is physically impossible, so if a sonde or
satellite VMR falls outside of these limits at any level, that profile is removed from the analysis. MLS only measures ozone
190 in the upper troposphere and above, so the ozonesonde concentrations within the troposphere are compared to the distribution
of the TROPES satellite ozone profiles. For each satellite-sonde set (e.g., AIRS + sondes), each sonde profile is compared to
the mean ± 5 standard deviations of the distribution of satellite profiles. If any concentrations in the sonde profile fall outside
of this range, the profile is removed from the analysis. This process is performed in the troposphere for each set of matched
satellite-sonde profiles. Using this method of QC, the percentage of profiles removed from CrIS, AIRS, and joint AIRS+OMI
195 comparisons are 4.5%, 3.5%, and 5.7%, respectively.

The number of matched, filtered data points for each satellite product at each sonde launch site is given in Fig. 2b. The
differences in the number of matched data points between satellite products is due to the differences in sampling, satellite data
throughput, and time period of data collection (see Sect. 2.1.1-2.1.3).

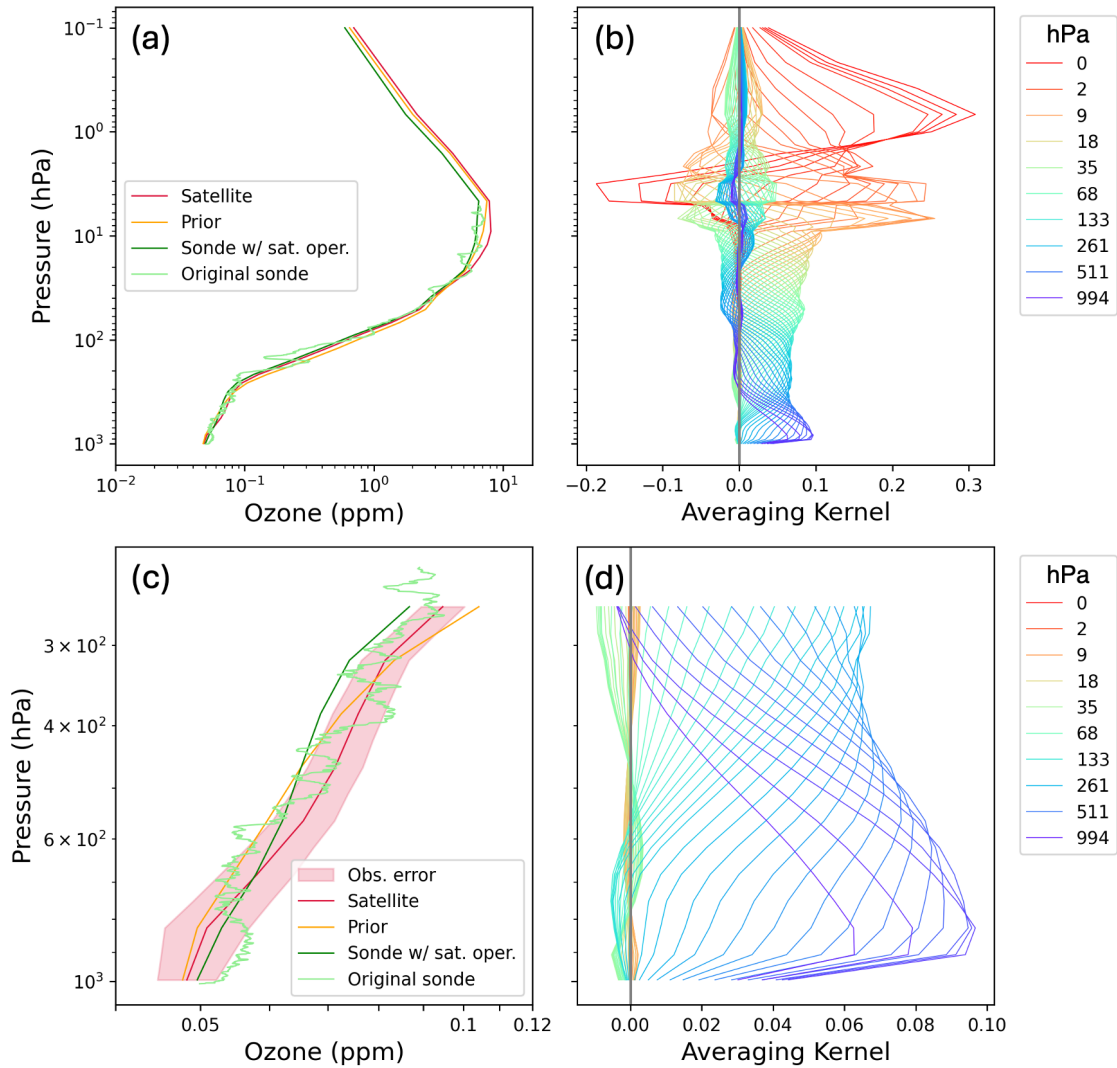


Figure 3. Example ozone profiles and averaging kernels from a comparison of a CrIS retrieval to an ozonesonde. (a) Ozone profile retrieved from the satellite (red), prior profile used in the CrIS retrieval (orange), profile measured by the ozonesonde (light green), and profile produced when the satellite operator is applied to the ozonesonde measurement (dark green). (b) Averaging kernel corresponding to the same retrieval in A. (c,d) Same as (a,b) with the vertical extent cropped to focus on the troposphere. The red shading in (c) indicates the observation error of the satellite profile.

2.3 Column calculations

200 The MUSES algorithm method is used to calculate total ozone columns and ozone subcolumns. The total ozone column is calculated by integrating the ozone from the surface to the top of the atmosphere — the highest-altitude point in the TROPESS

products, around 0.1 hPa. Calculating a subcolumn requires the definition of the maximum and minimum pressure levels for the column, as well as temperature and water vapor profiles to account for factors such as the Bernoulli equation and deviation from the ideal gas law. Temperature and water vapor profiles are provided by the TROPESS project (NASA, 2024).

205 Tropospheric columns are integrated from the surface to the thermal tropopause, as defined by the World Meteorological Organization (WMO) (WMO, 1957). The thermal tropopause is obtained from version 5 of the NASA Global Modeling and Assimilation Office (GMAO) Goddard Earth Observing System (GEOS-5) model Forward Processing for Instrument Teams (FP-IT) (Molod et al., 2012; GMAO, 2024; Lucchesi, 2015) and is specific to the date, time, and location of each data point. TROPESS defines the lower tropospheric column to extend from the surface to 500 hPa, and the upper tropospheric column to
210 extend from 500 hPa to the tropopause.

2.4 Correlation and trend analysis

The percent bias is calculated for every profile, column, and subcolumn according to Equation 2,

$$Percent\ Bias = \frac{C_{satellite} - C_{sonde}}{C_{sonde}} * 100\% \quad (2)$$

215 The calculation of trends follows guidance presented by the TOAR-II statistics focus working group (Chang et al., 2023). In brief, we use quantile regression (QR) to report trends at the 50th percentile. In comparison to other trend detection methods, QR is preferred due to its robustness to small sample sizes and outliers and its ability to account for non-normal error distributions and autocorrelation. The TOAR-II guidance also provides a method for moving block bootstrapping that we use to calculate the uncertainty of trends and assign a p-value to communicate the likelihood that a trend exists. Moving block
220 bootstrapping calculates the standard error of the trend over multiple subsamples ("blocks") along a time series, and is used to accurately quantify the trend uncertainty while taking autocorrelation and heteroskedasticity into account (Chang et al., 2023). Satellite-sonde correlation coefficients (r^2) are calculated using simple linear regression. To explore the geographic variability of ozone levels and data quality, results are grouped by latitude bands that are spaced every 30°.

3 Results

225 3.1 Satellite-sonde comparisons

The satellite and sonde profiles matched for each satellite product (Fig. S6) were used to derive profiles of percent difference for the three TROPESS products globally and within each latitude band (Fig. 4). The global mean percent bias profiles all fall within 20% bias, with the vertical distribution of bias varying by product. Each satellite instrument has a different vertical sensitivity, as indicated by the averaging kernels (Fig. 3 and S4), which results in differences in the ozone vertical profile.
230 However, because each satellite operator has been applied to each sonde profile, the biases primarily reflect differences in the air mass sampled within the coincidence criteria along with systematic and random errors in the satellite retrievals. The magnitude and vertical distribution of bias varies across latitude bands, but there is more variability across instruments than

across latitude for each instrument. Figure 4 illustrates the high volume of data in the Northern mid and high latitudes compared to the tropics and Southern Hemisphere, due to the lack of ozonesonde data in the Southern Hemisphere.

235 The TOB is represented by tropospheric column ozone (Fig. 1), so we calculate the percent bias between matched satellite- and sonde-measured columns. A time series of monthly averaged percent bias between matched satellite and sonde tropospheric ozone columns between 30 and 60°N is shown in Fig. 5a. The 50th percentile (i.e., median) of all of the points is given in the legend for each satellite product, and is displayed in the left-hand bar chart (Fig. 5b) for all latitude bands. All three satellite products tend to overestimate tropospheric ozone columns in all latitude bands, with AIRS having the lowest positive bias. 240 Joint AIRS+OMI tends to have the largest median bias, but the CrIS median bias can be of a comparable magnitude to joint AIRS+OMI (e.g., Fig. 5b 60-90°N). The median percent bias at each sonde site is given in Fig. S7S7a. The median bias is positive at most sites, but there are some negative median bias values. There can be large differences in the bias of the three products at some sites, and even sites within the same latitude band do not necessarily show consistent biases. The same analysis as shown in Fig. 5 but using absolute bias (in Dobson Units) is shown in Fig. S8.

245 To better understand the differences in satellite bias between products, the 50th percentile percent bias for each latitude band in both the lower troposphere (LT) and upper troposphere (UT) is given in Fig. 6. The largest overpredictions are in the UT, where satellite sensitivity tends to be larger (Fig. S4). The distribution of bias in the UT across latitude bands is consistent with the overall tropospheric column bias. In the LT, AIRS' and CrIS' bias fluctuates around 0 DU. AIRS and CrIS have lower sensitivities in the LT, so there is little true information in this altitude range and the lack of bias primarily reflects the use of 250 the same prior profile in both the satellite measurements and the sonde measurements with the satellite operator applied. Joint AIRS+OMI has greater sensitivity in the LT than the other two products, and it also tends to have the largest magnitude bias; it is negative at high northern latitudes, but positive in all other regions.

The TROESS products' tropospheric ozone biases are similar to the bias between other satellite products and ozonesondes. The mean tropospheric column ozone bias between the Tropospheric Emission Spectrometer (TES) and ozonesondes was 255 shown to range from 7 to 15% (Verstraeten et al., 2013) or approximately 2.9 DU (Osterman et al., 2008), with the UT displaying a wider range of bias than the LT (Nassar et al., 2008; Verstraeten et al., 2013). Our results show a decreased tropospheric column bias compared to TES (Fig. 5b), with a consistent distribution of bias between the UT and LT compared to TES. Whereas the three satellite products studied in this work display positive mean biases in most locations, other satellites display negative biases in some latitude bands. Boynard et al. (2018) showed that the IASI (Infrared Atmospheric Sounding 260 Interferometer)/Metop-A (IASI-A) and IASI/Metop-B (IASI-B) tropospheric ozone products had mean biases compared to sondes ranging 4-5% in high latitudes, -4 to -5% in midlatitudes, and -16 to -19% in the tropics. The OMI/MLS product presented by Ziemke et al. (2019) reported a mean bias of -2 DU for the tropospheric column ozone compared to global ozonesondes between 60°N and 60°S. Miles et al. (2015) showed a mean bias of approximately 10% (2 DU) in the Northern Hemisphere and -15 to -20% (-1 to -3 DU) in the Southern Hemisphere for the Global Ozone Monitoring Experiment 2 265 (GOME-2) RAL (Rutherford Appleton Laboratory) ozone retrieval. The median bias of the GOME-2 RAL product compared to sondes in the lower troposphere is approximately -1 DU (-6%) globally, -0.5 DU (-3%) in the NH, and 0 DU in the SH (Pope et al., 2023). Pope et al. (2023) also quantified the bias of the RAL GOME-1, OMI, and SCIAMACHY lower tropospheric

ozone columns compared to ozonesondes. The median bias of RAL GOME-1 is -5 DU (-26%) globally, -5 DU (-26%) in the NH, and -1 DU (-7%) in the SH; the median bias of RAL OMI is -4 DU (-19%) globally, -5.5 DU (-24%) in the NH, and -3.5 DU (-19%) in the SH; and the median bias of RAL SCIAMACHY is 2 DU (12%) globally, 2 DU (11%) in the NH, and 3.5 DU (28%) in the SH. While the sign of the mean biases can vary between satellite products, the absolute values are of approximately the same order of magnitude, suggesting that the TROPES products are of a similar quality as existing satellite products. Gaudel et al. (2018) calculated a mean TOB of 301 Tg with a range of 281-318 Tg across five satellite products. The 37 Tg range is equivalent to approximately $\pm 6\%$ of the average TOB. The differences in satellite-sonde bias across satellite products, ranging from -3 to 3 DU as shown in our results and the previous studies summarized here, likely accounts for at least some of the difference in measured TOB presented in Gaudel et al. (2018).

3.2 Trends in satellite-sonde bias

The time series of tropospheric ozone column biases (such as that shown in Fig. 5a) is used to calculate the trend in satellite-sonde bias and its uncertainties. The trends for each product are shown in the legend of Fig. 5a and for all latitude bands in Fig. 5c. Figure S8 displays the trends in concentration units (DU decade^{-1}) and Fig. S7-S7b displays the trends for each sonde launch site. The trend in satellite-sonde bias is within $\pm 2\%$ decade^{-1} for all products globally. Gulev et al. (2021) reported regional TOB trends ranging from 2 to 14% decade^{-1} (1-6 ppbv decade^{-1}). Globally, the trends in bias fall below the low end of that range (2% decade^{-1}) by a factor of 1-10.

When reported in each latitude band, the magnitude of the bias trend tends to be larger and the sign can vary. In most regions, the standard error on the trend (represented by the black lines in Fig. 5c) is larger than the trend itself and the p-values are large (Table S4). This suggests that the trends have very low certainty and cannot be distinguished from a trend of zero, and thus should not influence TOB trend detection. This is not true in the tropics, however, where there are relatively larger trends and smaller errors. This feature is investigated further in Sect. 3.3. A previous study comparing IASI-A and IASI-B to ozonesondes found an average drift of -8.6 (± 3.4) % decade^{-1} (-2.81 (± 1.26) DU decade^{-1}) in the Northern Hemisphere (Boynard et al., 2018). The TROPES products all have drift values less than that value, excluding CrIS in the tropics. Because most of the sonde data is collected in Northern mid-latitudes, the global average satellite-sonde bias is most strongly influenced by the data in those latitude bands. The bias trends reported in the 60°S - 30°S band were calculated using data at only one ozonesonde site: Lauder, New Zealand (Fig. 2). While this data may not be representative of the entire latitude band, we choose to include the results because the Lauder site has a relatively high data volume and is an important source of data in the Southern Hemisphere (Fig. 2b). Additionally, the profiles of satellite-sonde bias at the Lauder site (Fig. 4p-r) display similar features as the profiles in other latitude bands, suggesting that the Lauder site provides meaningful data. The ability of one site to represent trends throughout a region is discussed further in Sect. 4.

To further investigate the spatial distribution of biases in satellite retrievals, we quantify the correlation between the satellite-sonde biases at different sonde launch sites. If the monthly time series of percent bias at different sites are uncorrelated, then the satellite products are providing geographically independent data. As an example, the bias time series at one site (e.g., Uccle, Belgium) was compared to the bias time series at a second site (e.g., Valentia, Ireland), and the r^2 between the time

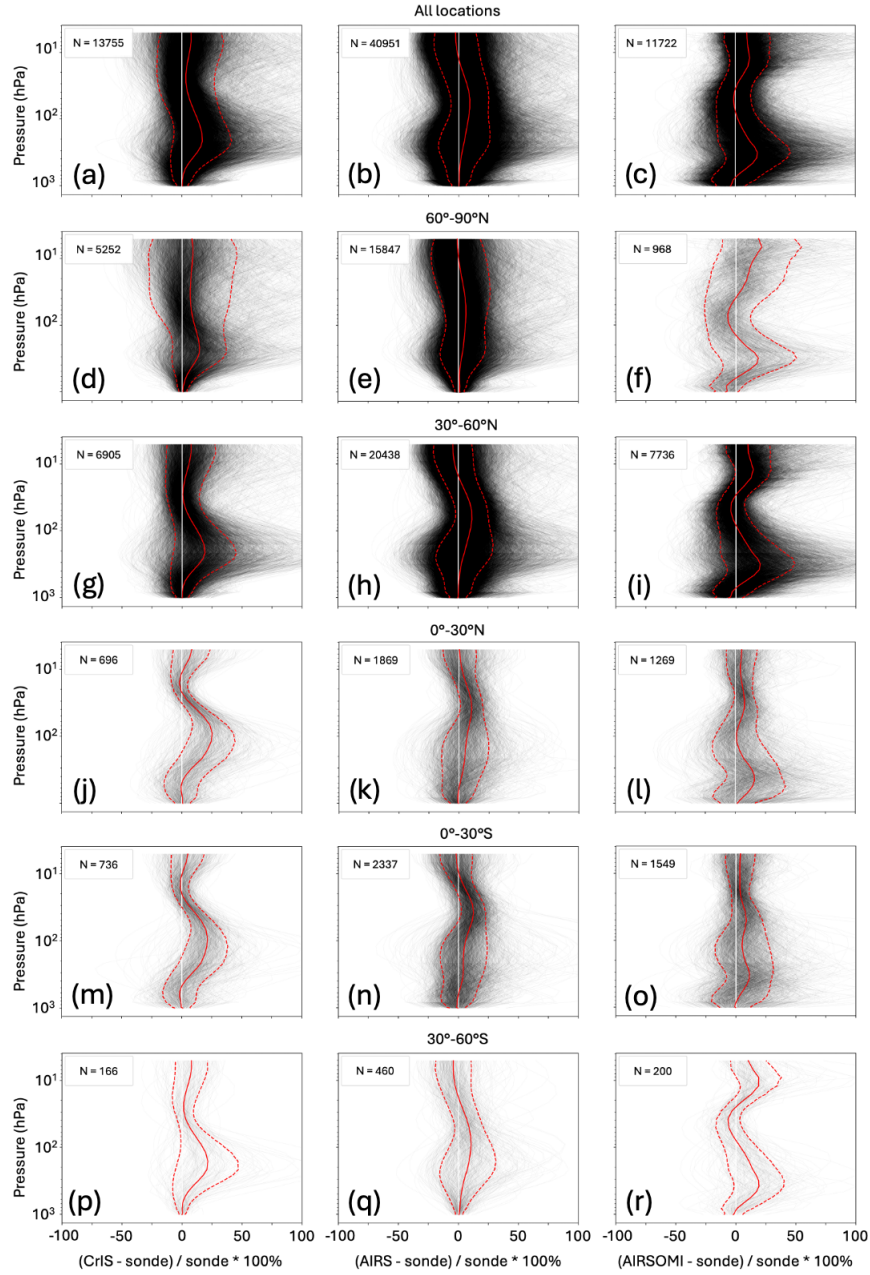


Figure 4. Percent bias between each matched satellite and sonde profile for CrIS (left), AIRS (center), and joint AIRS+OMI (right). The top row includes data at all sites, and subsequent rows contain data in each 30°latitude band. The solid red lines represent the mean difference profile and the dashed red lines represent one standard deviation away from the mean. The number of profiles in each latitude band is indicated by the density of the individual black lines. The solid white lines are at 0%.

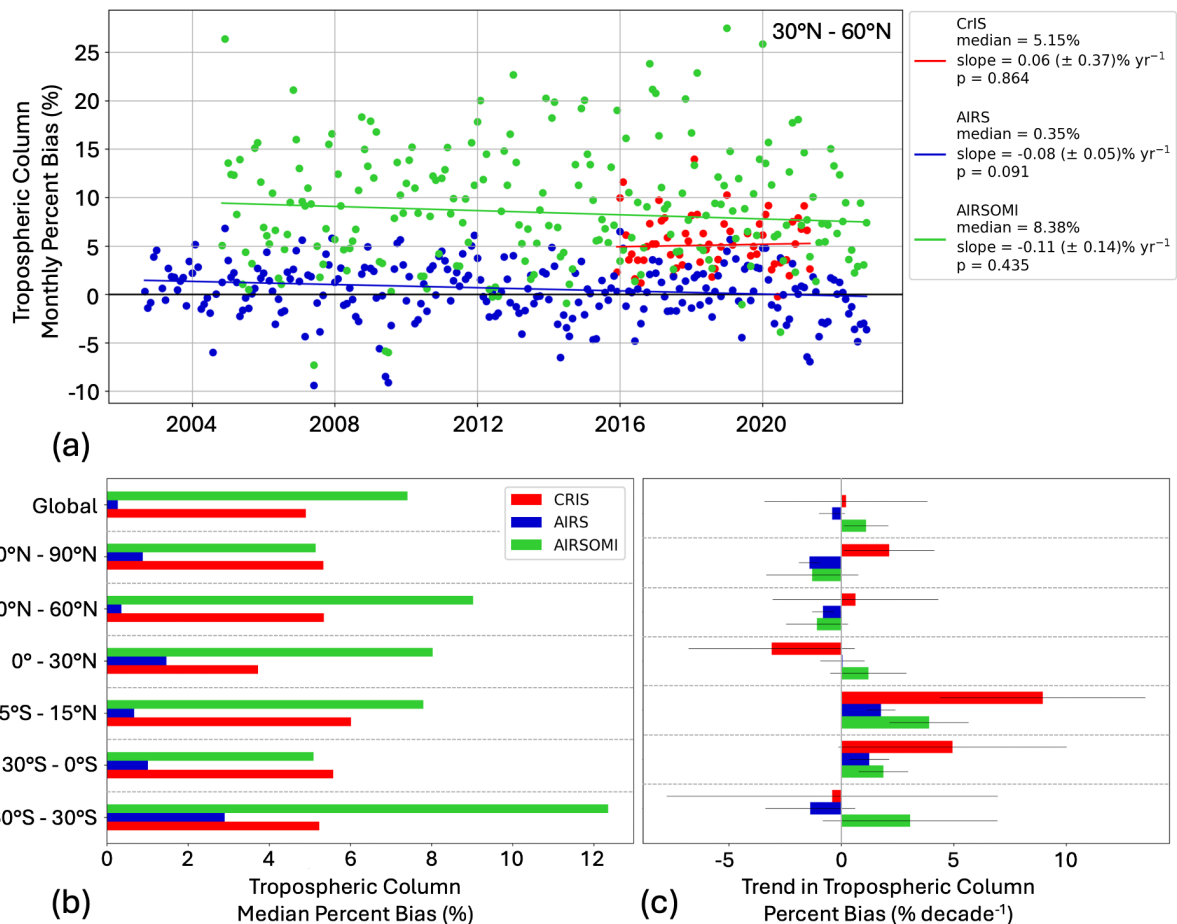


Figure 5. Top: Monthly-averaged tropospheric column percent bias for all sites between 30°N and 60°N. The slope, standard error of the slope, and p-value of the slope are reported for the 50th percentile. The medians and slopes reported in the bottom row are derived from time series such as this. Bottom left: The median tropospheric column percent bias in each latitude band. Bottom right: The trend in tropospheric column percent bias in each latitude band. There are no sonde sites between 60°S and 90°S.

series data was calculated. This analysis was performed between all pairs of sites and the r^2 values are given in Fig. S9. High r^2 values indicate a relationship between the bias in different locations, while a low r^2 value indicates no relationship. The r^2 values are consistently low between sites, even sites that are in similar regions such as mainland Europe (De Bilt, Valentia, Uccle, Hohenpeissenberg, Payerne, L'Aquila, and Madrid) ,Costa Rica (Alajuela and Heredia), or Brazil (Natal and Maxaranguape or western North America (Trinidad Head, Port Hardy, Kelowna, and Edmonton)). This suggests that satellite-sonde bias is random and not systematic by location. While the sonde sites do not represent the entire globe and are not evenly distributed, this preliminary analysis suggests that the satellite performance is not strongly location-dependent.

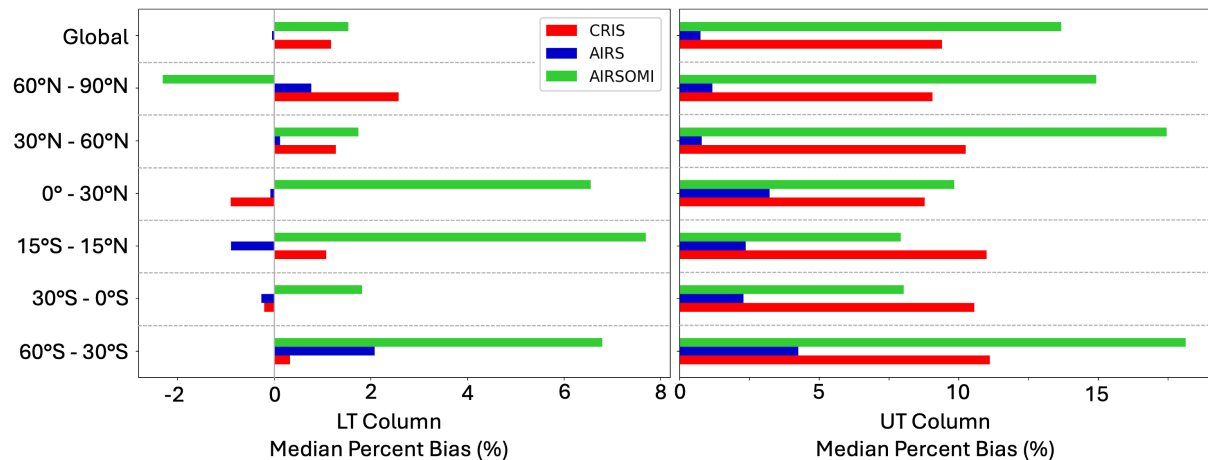


Figure 6. The median LT (left) and UT (right) column percent bias averaged over sites in each latitude band. There are no sonde sites between 60°S and 90°S.

The satellite products cover different time periods, with CrIS providing data for the shortest time period. To compare the products during only their overlapping time periods, the AIRS and joint AIRS+OMI data were cropped to the same time period as CrIS and the median percent bias and the trend in the percent bias were calculated in the same manner as Fig. 5 (see Fig. S10). The change in the median percent bias between the two time periods was minor at almost all sites, but the magnitude of the trend in the bias increased at many sites. At the same time, the standard errors of the trends tend to be larger than the trends themselves and many of the p-values are large (i.e., over 0.33; Fig. S10), meaning that the trends in bias during this time period are uncertain and may not be differentiable from 0 (Chang et al., 2023). The large errors highlight the difficulty of trying to determine a trend over a short time period, particularly for a trace gas with large interannual variability like tropospheric ozone. While one may be tempted to infer that these 2015-2021 bias trends indicate the current performance of the AIRS and joint AIRS+OMI satellite products, the uncertainty of the trends suggests that 5 years is not a sufficient period for trend detection. The results also imply that the relatively large trends in bias seen in CrIS as compared to the other two instruments are primarily driven by the short length of the record rather than by any instability or deficiency in the CrIS product.

3.3 Seasonal dependence of biases

The seasonal dependence of tropospheric, UT, and LT column satellite-sonde comparisons is shown in Fig. 7. Seasonal dependencies arise in CrIS and AIRS because they are both TIR instruments and thus their sensitivity to ozone depends on the thermal structure of the atmosphere, particularly the thermal contrast between the surface and the lowest layer of the atmosphere. The sensitivity of OMI likewise varies with season, as it depends strongly on solar insolation. As expected, AIRS and CrIS have similar seasonal patterns, with the smallest standard deviations in SON and the largest standard deviations in DJF. The seasonal spread of AIRS and CrIS is relatively small in the LT, likely because of their low sensitivity there, with most of

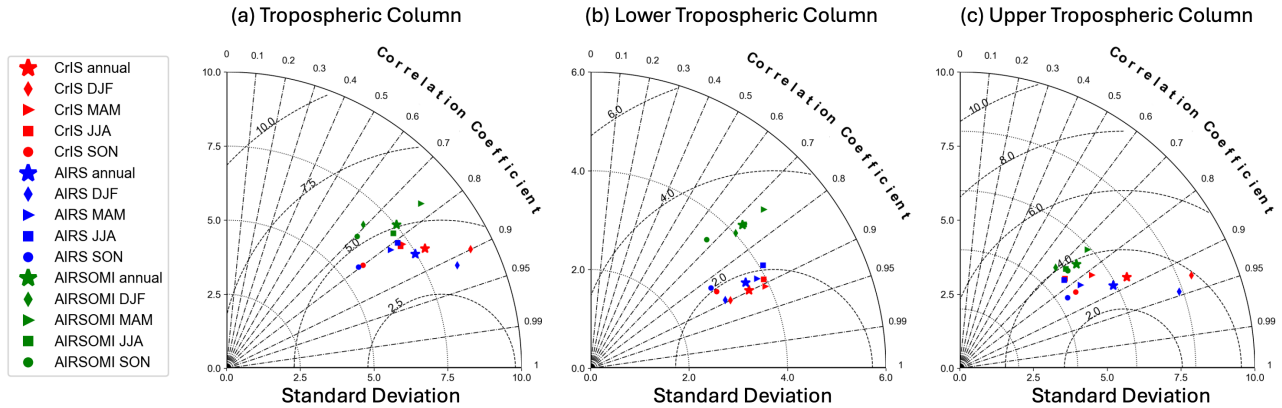


Figure 7. Taylor diagram representing global statistics of CrIS (red), AIRS (blue), and joint AIRS+OMI (green) tropospheric column comparisons with sondes. The radial distance from the origin represents standard deviation, azimuthal angle represents the correlation coefficient (r), and the dashed arcs centered on the x-axis represent the root mean square error (RMSE). Markers represent datasets in each season (DJF: December/January/February, MAM: March/April/May, JJA: June/July/August, SON: September/October/November) and annually.

the seasonal differences occurring in the UT. High standard deviations in the UT in DJF are caused by high ozone values (Fig. S11) occurring in the Northern high latitudes (Fig. S12). Figures S11-S12 are presented for AIRS, but similar ozone distributions are seen in the CrIS dataset. The joint AIRS+OMI product has low data volume near the poles and does not properly capture the long tail of the ozone distribution in Northern high latitudes. Because the high ozone values are seen in both the satellite records and the sondes, they are likely to be real. Previous work used the Modern-Era Retrospective analysis for Research and Applications Version 2 (MERRA-2) global reanalysis model to show the prevalence of multiple tropopauses at high Northern latitudes (Manney et al., 2017). Multiple tropopauses often form when upper tropospheric jets impinge on the high-altitude tropopause in the tropics, causing high-altitude tropospheric air to "bend" poleward into regions with lower-altitude tropopauses (Manney et al., 2014). Multiple tropopauses allow for enhanced mixing between the troposphere and stratosphere, allowing for high stratospheric ozone concentrations to intrude into the troposphere and raise ozone concentrations. Manney et al. (2017) also found a high frequency of multiple tropopauses in high Southern latitudes in JJA, but we do not observe high ozone values in JJA in the TROPESS datasets due to the lack of coincident satellite and sonde measurements below 60°S.

Figure 7 also demonstrates that joint AIRS+OMI has the lowest correlation with sonde measurements in all vertical regimes, with the largest difference between joint AIRS+OMI and the other two satellite products in the LT. Joint AIRS+OMI has the highest sensitivity in the LT compared to AIRS and CrIS (see Fig. S4) because it includes UV radiances from OMI, which are sensitive to the entire ozone column, including the surface (Fu et al., 2018). While it is clear that there is a systematic bias in the LT TROPESS joint AIRS+OMI retrievals, the relative lack of bias in AIRS and CrIS likely arises because their retrievals provide little information in the LT due to low sensitivity. Since the satellite operator is applied to the ozonesonde measurements, this lack of sensitivity results in both the retrieved satellite and sonde profiles largely reverting to the prior values.

The satellite-sonde percent bias also varies across season (Tables 2, 3, 4). In the Northern Hemisphere, the bias is largest for all three products in DJF and smallest in JJA. This seasonal pattern is also reflected in the global values since most of the data falls in the Northern Hemisphere. In the Southern Hemisphere, the change in bias across seasons is less consistent, but this may be due to the lack of data in the Southern Hemisphere compared to the Northern Hemisphere. In all seasons, the CrIS and joint AIRS+OMI biases remain positive (except 30-60°S CrIS in DJF), whereas the AIRS bias is negative in the spring (MAM) and summer (JJA) in the Northern Hemisphere and spring (SON) in the Southern Hemisphere.

Seasonality is also seen in the trend in satellite-sonde bias and can explain why the trend in tropical percent bias is larger than that in other regions (Tables 2, 3, 4). There is little consistency in the seasonality of the bias trend across products, but it is noteworthy that the magnitudes of the seasonal bias trends are substantially larger for CrIS than the annual average trend in most regions. However, we caution against over-interpreting these results given the relatively short duration of the CrIS product. In many regions, the bias trend fluctuates between positive and negative values across seasons, resulting in a small annual average value for each product. But in the tropics (15°S-15°N), the bias trend is almost always positive, leading to the large trend in annual bias, particularly for CrIS (Fig. 5c). The satellite sensitivity to ozone tends to be largest in the tropics due to a combination of good thermal contrast, warm atmospheric temperatures, high insolation, and large ozone abundances. The variability in these parameters is also lowest in the tropics, so that the sensitivity is more likely to be consistent across seasons. The seasonal dependence of the biases and how they vary across region and for each satellite product are important to consider when quantifying a trend in only one season or month. For example, some studies quantify the tropospheric ozone trend in summer only, since summer typically has the highest ozone values and worst air pollution. The impact of time-dependent satellite bias can be different in the summer season than for the annual average, so the bias in each time frame should be considered explicitly.

Table 2: Comparisons between CrIS and sonde tropospheric ozone columns: sample size (N), bias (%), trend (% decade⁻¹), error (standard error on the trend), and p-value on the trend. Data are separated by region and season.

| | CrIS | | | | | | | | | |
|---------|-----------|------|------|------|------|-----------|------|------|------|-------|
| | all dates | DJF | MAM | JJA | SON | all dates | DJF | MAM | JJA | SON |
| | 60°-90°N | | | | | 30°-60°N | | | | |
| N | 5252 | 1894 | 1393 | 915 | 1050 | 6905 | 2112 | 1664 | 1320 | 1809 |
| bias | 5.0 | 6.5 | 3.8 | 3.7 | 5.2 | 5.2 | 7.3 | 6.0 | 2.7 | 4.1 |
| trend | 2.1 | -4.5 | -3.6 | 0.75 | 4.2 | 0.63 | -4.6 | 2.0 | 0.57 | -0.61 |
| error | 2.0 | 5.4 | 5.6 | 4.6 | 5.1 | 3.7 | 5.5 | 5.8 | 6.1 | 3.7 |
| p-value | 0.30 | 0.42 | 0.52 | 0.87 | 0.42 | 0.86 | 0.42 | 0.74 | 0.93 | 0.87 |
| | 0°-30°N | | | | | 15°S-15°N | | | | |
| N | 696 | 221 | 155 | 146 | 174 | 958 | 271 | 238 | 238 | 211 |
| bias | 3.7 | 4.7 | 4.2 | 4.1 | 1.2 | 5.1 | 5.0 | 6.0 | 4.5 | 4.0 |
| trend | -3.1 | 3.3 | -8.4 | 0.75 | 1.3 | 9.0 | 7.2 | 8.1 | 19.2 | 5.9 |

| | | | | | | | | | | |
|---------|----------------|-------|------|------|-------|-----------------|-------|------|------|------|
| error | 3.7 | 9.3 | 9.4 | 11.1 | 8.8 | 4.6 | 10.8 | 8.0 | 9.9 | 8.2 |
| p-value | 0.40 | 0.73 | 0.38 | 0.95 | 0.88 | 0.05 | 0.51 | 0.33 | 0.07 | 0.48 |
| | 0°-30°S | | | | | 30°-60°S | | | | |
| N | 736 | 174 | 192 | 192 | 178 | 166 | 57 | 39 | 30 | 40 |
| bias | 4.5 | 5.8 | 3.7 | 5.3 | 3.7 | 4.34 | -0.07 | 4.2 | 8.0 | 1.5 |
| trend | 4.9 | -0.26 | 0.60 | 4.6 | -12.5 | -0.40 | 1.8 | 0.83 | 6.9 | 0.10 |
| error | 5.1 | 14.6 | 16.9 | 17.7 | 8.1 | 7.4 | 32.8 | 16.6 | 22.2 | 23.7 |
| p-value | 0.33 | 0.99 | 0.97 | 0.80 | 0.14 | 0.96 | 0.96 | 0.96 | 0.76 | 1.0 |
| | global | | | | | | | | | |
| N | 13755 | 4458 | 3443 | 2603 | 3251 | | | | | |
| bias | 4.8 | 7.1 | 5.1 | 3.0 | 4.1 | | | | | |
| trend | 0.21 | -1.0 | 1.0 | 3.3 | 0.82 | | | | | |
| error | 3.6 | 2.6 | 4.3 | 3.5 | 3.9 | | | | | |
| p-value | 0.95 | 0.70 | 0.81 | 0.36 | 0.83 | | | | | |

Table 3: Same as Table 2 but for AIRS.

| | | | | | | | | | | |
|---------|-----------------|------|-------|-------|------|------------------|------|-------|-------|-------|
| | AIRS | | | | | | | | | |
| | all dates | DJF | MAM | JJA | SON | all dates | DJF | MAM | JJA | SON |
| | 60°-90°N | | | | | 30°-60°N | | | | |
| N | 15847 | 5410 | 4131 | 2892 | 3414 | 20438 | 4683 | 5127 | 5296 | 5332 |
| bias | 0.80 | 2.4 | -0.52 | -1.1 | 2.5 | 0.35 | 2.8 | -0.47 | -1.1 | 0.63 |
| trend | -1.4 | -1.7 | 0.30 | -1.3 | -1.8 | -0.82 | -1.2 | 0.06 | -0.26 | -1.5 |
| error | 0.46 | 0.65 | 0.65 | 0.63 | 0.91 | 0.48 | 0.73 | 0.82 | 0.73 | 1.0 |
| p-value | 0.002 | 0.01 | 0.65 | 0.04 | 0.05 | 0.09 | 0.11 | 0.95 | 0.72 | 0.16 |
| | 0°-30°N | | | | | 15°S-15°N | | | | |
| N | 1869 | 451 | 421 | 503 | 494 | 2697 | 629 | 597 | 763 | 708 |
| bias | 1.0 | 1.2 | 1.9 | -0.01 | 0.97 | 0.79 | 1.6 | 1.5 | 0.20 | -0.33 |
| trend | 0.06 | -1.2 | -0.34 | -0.29 | 1.8 | 1.8 | 0.77 | 2.4 | 2.9 | -0.01 |
| error | 0.99 | 1.4 | 1.9 | 2.0 | 1.6 | 0.64 | 0.89 | 1.0 | 1.4 | 1.8 |
| p-value | 0.95 | 0.37 | 0.86 | 0.89 | 0.29 | 0.01 | 0.39 | 0.02 | 0.04 | 0.99 |
| | 0°-30°S | | | | | 30°-60°S | | | | |
| N | 2337 | 507 | 561 | 700 | 569 | 460 | 90 | 123 | 113 | 134 |
| bias | 0.98 | 1.2 | 2.1 | 0.85 | 0.24 | 1.8 | 1.9 | 0.07 | 7.4 | -0.67 |

| | | | | | | | | | | |
|---------|---------------|-------|-------|------|------|------|-------|------|-------|------|
| trend | 1.2 | -0.99 | 1.7 | 3.4 | 1.6 | -1.4 | -0.91 | -7.1 | -0.53 | 0.21 |
| error | 0.88 | 1.6 | 1.1 | 1.3 | 2.2 | 2.0 | 5.5 | 3.0 | 3.0 | 3.9 |
| p-value | 0.16 | 0.54 | 0.13 | 0.01 | 0.46 | 0.49 | 0.87 | 0.02 | 0.86 | 0.96 |
| | global | | | | | | | | | |
| N | 43735 | 11141 | 10363 | 9504 | 9943 | | | | | |
| bias | 0.36 | 2.2 | -0.58 | -1.2 | 1.0 | | | | | |
| trend | -0.41 | -0.58 | 0.19 | 0.17 | -1.5 | | | | | |
| error | 0.57 | 0.58 | 0.68 | 0.54 | 0.87 | | | | | |
| p-value | 0.48 | 0.32 | 0.78 | 0.75 | 0.08 | | | | | |

Table 4: Same as Table 2 but for joint AIRS+OMI.

| | | | | | | | | | | |
|---------|-----------------------|-------|------|-------|------|------------------|-------|-------|------|-------|
| | Joint AIRS+OMI | | | | | | | | | |
| | all dates | DJF | MAM | JJA | SON | all dates | DJF | MAM | JJA | SON |
| | 60°-90°N | | | | | 30°-60°N | | | | |
| N | 968 | 93 | 247 | 410 | 218 | 7736 | 843 | 1804 | 3052 | 2037 |
| bias | 4.8 | 12.3 | 1.8 | -0.17 | 7.3 | 8.4 | 13.5 | 9.1 | 2.8 | 9.5 |
| trend | -1.3 | -0.70 | -2.2 | 1.7 | -4.1 | -1.1 | 0.97 | -0.31 | 1.9 | -2.6 |
| error | 2.0 | 4.3 | 3.9 | 2.7 | 2.7 | 1.4 | 1.3 | 1.3 | 0.99 | 1.8 |
| p-value | 0.53 | 0.87 | 0.57 | 0.54 | 0.14 | 0.44 | 0.47 | 0.82 | 0.06 | 0.15 |
| | 0°-30°N | | | | | 15°S-15°N | | | | |
| N | 1269 | 222 | 283 | 416 | 348 | 1759 | 343 | 414 | 518 | 484 |
| bias | 7.5 | 11.7 | 5.9 | 6.3 | 5.5 | 6.3 | 10.3 | 8.8 | 5.4 | 4.2 |
| trend | 1.2 | 0.46 | 3.5 | 3.4 | -1.7 | 3.9 | 8.0 | 2.9 | 5.9 | -0.47 |
| error | 1.7 | 3.1 | 3.1 | 2.3 | 2.9 | 1.8 | 3.2 | 2.8 | 2.2 | 2.0 |
| p-value | 0.48 | 0.88 | 0.26 | 0.16 | 0.55 | 0.03 | 0.02 | 0.31 | 0.01 | 0.82 |
| | 0°-30°S | | | | | 30°-60°S | | | | |
| N | 1549 | 288 | 397 | 435 | 429 | 200 | 63 | 67 | 28 | 42 |
| bias | 4.7 | 3.2 | 6.7 | 5.3 | 2.5 | 11.7 | 9.1 | 17.2 | 13.7 | 9.7 |
| trend | 1.9 | 3.6 | 1.8 | 1.7 | -1.3 | 3.1 | -0.16 | 7.4 | -2.6 | 8.0 |
| error | 1.1 | 2.4 | 1.9 | 1.4 | 1.6 | 3.9 | 7.6 | 4.9 | 8.5 | 7.8 |
| p-value | 0.09 | 0.13 | 0.36 | 0.22 | 0.40 | 0.43 | 0.98 | 0.14 | 0.77 | 0.31 |
| | global | | | | | | | | | |
| N | 11722 | 1509 | 2798 | 4341 | 3074 | | | | | |

| | | | | | |
|---------|------|------|------|------|------|
| bias | 6.8 | 11.5 | 7.2 | 3.4 | 7.4 |
| trend | 1.1 | 3.5 | 1.3 | 1.6 | -1.5 |
| error | 1.0 | 1.2 | 1.4 | 0.89 | 1.2 |
| p-value | 0.27 | 0.00 | 0.36 | 0.08 | 0.22 |

4 Discussion

The focus of this study was to comprehensively compare TROPESS tropospheric ozone products to ozonesonde data by quantifying satellite-sonde biases and their evolution with time. Nonetheless, we wish to emphasize that analyses must consider the time range used for trend detection, as a short time period may not provide enough information to detect trends with high precision. The CrIS dataset used here runs from late 2015 to mid 2021, and the uncertainty associated with the CrIS-sonde bias trends are high (Fig. 5 and Table S4), except in the tropics. Additionally, when the AIRS and joint AIRS+OMI datasets were cropped to the same time period as the CrIS record, the uncertainties on their bias trends were very large as well. The ability to quantify a drift with high precision depends on both the magnitude of the drift and its variability, with longer records required for smaller drifts and/or larger variability. It is critical that statistical methods such as block bootstrapping, which preserves the correlation between consecutive data points and therefore more accurately captures the variance of a time series than other methods, are used to assess statistical significance and determine whether a given record is long enough to detect a trend.

A substantial portion of the effort underlying this analysis was directed at establishing QC methods for the ozonesonde data (Sect. 2.2.2 and SI), and we wish to emphasize that this process can impact the outcome of validation (i.e., bias estimation) studies. While the ozonesonde data has low measurement uncertainty and has historically been used to represent "true" ozone values, some of the sonde data has poor quality or does not interact with the satellite operator in a physically realistic manner. In some cases, the ozonesonde concentrations are realistic in the stratosphere and not the troposphere, but the application of the satellite operator convolves the stratosphere and troposphere, making those profiles unusable. Typically, studies that utilize sonde data develop their own QC methods, especially when working with satellite operators from a variety of products. As shown in Sect. S1, the QC methods and subset of sonde data used can impact the quantification of satellite-sonde bias. So studies that use different QC methods may not be comparing their datasets to the same "true" information.

Section S1 suggests important topics for users of sonde data to consider when comparing to satellite ozone products. First, sonde users should investigate the impact that QC methods have on their results. This is true for ozone trend studies and studies that quantify instrument bias using sonde data as the ground truth dataset. As illustrated in Sect. S1, the trend in satellite-sonde bias varied by an order of magnitude and sign, ranging from -0.24 to 0.21% decade⁻¹ (Table S2), depending on the QC method selected. The median bias and trend in bias stabilized when certain methods were employed (Tables S2, S3), suggesting that some methods provide more realistic and stable metrics than other methods. In addition to considering the stability of the bias, users should also consider the vertical profile of the bias, as different methods resulted in more or less physically realistic profiles at different levels (Fig. S2). Second, applying QC methods to the original sonde data may not be sufficient to completely QC the data when working with satellite operators, since the application of the satellite operator can

introduce physically unrealistic behavior. On the other hand, studies focusing solely on the sonde data will need to apply QC methods to only the raw sonde data. Because observational operators vary by instrument and in both space and time, we cannot state that our optimal QC method is tailored for use with other datasets. Third, QC methods can use historical or modeled data (e.g., from satellites, ground-based systems, and global models) to provide physically realistic concentration limits. In this study, the MLS climatology provided a physical basis for the screening of unrealistic profiles in the stratosphere. Future work could investigate the curation of a long-term ozone climatology in the troposphere for use in QC screening. In summary, we recommend that future studies utilizing sonde data consider the impact of QC methods and how the chosen subset of sonde data compares to existing studies.

Another important consideration is whether the sonde sites are truly representative of global ozone and can be used to accurately quantify global satellite-sonde bias. The ozonesonde sites are mostly grouped in the Northern mid to high latitudes (Fig. 2 and 4), with little coverage in the Southern Hemisphere and most continents apart from Europe and North America. There is only one sonde site providing harmonized data between 60°S and 30°S (Lauder, New Zealand) and there is no harmonized sonde data available below 60°S. In this study, we used harmonized ozonesonde data provided by the HEGIFTOM group as part of the TOAR-II project (Van Malderen et al., 2025), which did not include data at all sonde sites at the time of production. For example, some data in East Asia had not yet been harmonized and this could limit our ability to evaluate satellite ozone performance over this region. Chang et al. (2024) showed that the sampling of hourly ozone measurements at the Mauna Loa Observatory could drastically impact the accuracy of long-term trend detection. This work also showed that small-scale meteorological variability affects the trends. These results were given at one site, but demonstrate the impact of localized phenomena on trend detection from *in situ* observations, suggesting that individual sites may not be representative of regional trends if their temporal sampling or meteorology are inconsistent. Future work will focus on assessing the degree to which the satellite-sonde intercomparisons shown here are representative of broader changes in bias using a tropospheric chemistry reanalysis (Miyazaki et al., 2020a, b).

This study suggests important considerations for the TOAR community when performing validation or trend analyses that compare multiple satellite products. In addition to the factors presented above (i.e., time range, sonde QC methods, and geographic representativeness), the sensitivity of the instruments, the *a priori* information, and other factors in the retrievals algorithms can impact trend detection. The TROPESS products used in this study were retrieved using a consistent algorithm that used the same *a priori* information, tropopause definitions, and vertical grids for all products. In an ideal scenario, all satellite products used in intercomparison studies would also use these consistent variables. Importantly, they would also all be compared to ozonesonde or other *in situ* data using the same filtering criteria, rather than comparing to a variable ground truth dataset. While this would require significant effort to accomplish the large number of available satellite products, these steps would allow for the most accurate comparison of satellite measurement error and quantification of tropospheric ozone.

5 Conclusions

This study compares long-term tropospheric ozone records from three satellite products and ozonesondes. The CrIS, AIRS, and joint AIRS+OMI products are those developed by the TROPESS project, which uses a common retrieval algorithm and consistent *a priori* information to provide ozone profiles with quantified uncertainties. A major goal of the TOAR-II project is to quantify long-term trends in tropospheric ozone, which requires understanding to what degree the observed trend is attributable to non-physical properties such as instrument measurement drift. The TROPESS products were compared to global ozonesonde data and the magnitude of the trends in satellite-sonde bias for the three products (CrIS: $0.21 \pm 3.6\%$ decade⁻¹, AIRS: $-0.41 \pm 0.57\%$ decade⁻¹, and joint AIRS+OMI: $1.1 \pm 1.0\%$ decade⁻¹) are approximately one order of magnitude less than the reported range in tropospheric ozone trends (-7.1% decade⁻¹ to 9.5% decade⁻¹). This work suggests that the three TROPESS products can be used to accurately detect global tropospheric ozone trends. Future work to quantify trends in specific regions or seasons, however, should consider the impact that more localized satellite measurement drift has on trend detection. While the measurement drift could not be quantified with high precision in many regions or seasons (Fig. 5 and Tables 2 - 4), the tropics displayed unique behavior with consistently positive and non-zero drift in all instruments.

Data availability. TROPESS satellite data is available at the NASA GES-DISC database (<https://disc.gsfc.nasa.gov/datasets?page=1&project=TROPESS>). TROPESS datasets with the complete set of variables are available by contacting the corresponding author. Information about acquiring harmonized ozonesonde data is available at <https://hegiftom.meteo.be/datasets/ozonesondes> (HEGIFTOM, 2024).

Author contributions. All authors conceptualized the project, provided technical guidance, and contributed to writing and editing the article. EAP performed data analysis and led the writing and editing of the article.

Competing interests. The authors have no competing interests to declare.

Acknowledgements. The authors would like to thank Roeland Van Malderan for providing and assisting with the ozonesonde data. We also thank Frank Werner for processing the MLS climatology data. The research was carried out at the Jet Propulsion Laboratory, California Institute of Technology, under a contract with the National Aeronautics and Space Administration (80NM0018D0004). We also acknowledge the support of the NASA Atmospheric Composition: Aura Science Team Program (19-AURAST19-0044), Earth Science U.S. Participating Investigator program (22-EUSPI22-0005), ACMAP (22-ACMAP22-0013), and the NASA TROPESS project.

References

- AIRS: AIRS/Aqua L1B Infrared (IR) geolocated and calibrated radiances V005, <https://doi.org/10.5067/YZEXEVN4JGGJ>, 2007.
- AIRS: Aqua/AIRS L2 Near Real Time (NRT) Standard Physical Retrieval (AIRS-only) V7.0, <https://doi.org/10.5067/RAEHAOH4VZM5>,
455 2019.
- Aumann, H., Chahine, M., Gautier, C., Goldberg, M., Kalnay, E., McMillin, L., Revercomb, H., Rosenkranz, P., Smith, W., Staelin, D., Strow, L., and Susskind, J.: AIRS/AMSU/HSB on the Aqua mission: design, science objectives, data products, and processing systems, *IEEE Transactions on Geoscience and Remote Sensing*, 41, 253–264, <https://doi.org/10.1109/TGRS.2002.808356>, conference Name: IEEE Transactions on Geoscience and Remote Sensing, 2003.
- 460 Barnet, C. D., Divakarla, M., Gambacorta, A., Iturbide-Sanchez, F., Nalli, N. R., Pryor, K., Tan, C., Wang, T., Warner, J., Zhang, K., and Zhu, T.: NOAA Unique Combined Atmospheric Processing System (NUCAPS): Algorithm Theoretical Basis Document, Tech. Rep. Version 3.1, NOAA NESDIS STAR, https://www.star.nesdis.noaa.gov/jpss/documents/ATBD/ATBD_NUCAPS_v3.1.pdf, 2021.
- Beer, R.: TES on the aura mission: scientific objectives, measurements, and analysis overview, *IEEE Transactions on Geoscience and Remote Sensing*, 44, 1102–1105, <https://doi.org/10.1109/TGRS.2005.863716>, conference Name: IEEE Transactions on Geoscience and Remote
465 Sensing, 2006.
- Bowman, K., Rodgers, C., Kulawik, S., Worden, J., Sarkissian, E., Osterman, G., Steck, T., Lou, M., Eldering, A., Shephard, M., Worden, H., Lampel, M., Clough, S., Brown, P., Rinsland, C., Gunson, M., and Beer, R.: Tropospheric emission spectrometer: retrieval method and error analysis, *IEEE Transactions on Geoscience and Remote Sensing*, 44, 1297–1307, <https://doi.org/10.1109/TGRS.2006.871234>, conference Name: IEEE Transactions on Geoscience and Remote Sensing, 2006.
- 470 Boynard, A., Hurtmans, D., Garane, K., Goutail, F., Hadji-Lazaro, J., Koukouli, M. E., Wespes, C., Vigouroux, C., Keppens, A., Pommereau, J.-P., Pazmino, A., Balis, D., Loyola, D., Valks, P., Sussmann, R., Smale, D., Coheur, P.-F., and Clerbaux, C.: Validation of the IASI FOR-LI/EUMETSAT ozone products using satellite (GOME-2), ground-based (Brewer–Dobson, SAOZ, FTIR) and ozonesonde measurements, *Atmospheric Measurement Techniques*, 11, 5125–5152, <https://doi.org/10.5194/amt-11-5125-2018>, publisher: Copernicus GmbH, 2018.
- Brewer, A. W., Milford, J. R., and Dobson, G. M. B.: The Oxford-Kew ozone sonde, *Proceedings of the Royal Society of London. Series A. Mathematical and Physical Sciences*, 256, 470–495, <https://doi.org/10.1098/rspa.1960.0120>, publisher: Royal Society, 1997.
475
- Chang, K.-L., Schultz, M. G., Koren, G., and Selke, N.: Guidance note on best statistical practices for TOAR analyses, https://igacproject.org/sites/default/files/2023-04/STAT_recommendations_TOAR_analyses_0.pdf, 2023.
- Chang, K.-L., Cooper, O. R., Gaudel, A., Petropavlovskikh, I., Effertz, P., Morris, G., and McDonald, B. C.: Technical note: Challenges in detecting free tropospheric ozone trends in a sparsely sampled environment, *Atmospheric Chemistry and Physics*, 24, 6197–6218,
480 <https://doi.org/10.5194/acp-24-6197-2024>, publisher: Copernicus GmbH, 2024.
- Dufour, G., Eremenko, M., Cuesta, J., Ancellet, G., Gill, M., Maillard Barras, E., and van Malderen, R.: Performance assessment of the IASI-O3 KOPRA product for observing midlatitude tropospheric ozone evolution for 15 years: validation with ozone sondes and consistency of the three IASI instruments, *Atmospheric Measurement Techniques Discussions*, <https://doi.org/10.5194/egusphere-2024-4096>, publisher: Copernicus Publications / European Geosciences Union, 2025.
- 485 Elshorbany, Y., Ziemke, J. R., Strode, S., Petetin, H., Miyazaki, K., De Smedt, I., Pickering, K., Seguel, R. J., Worden, H., Emmerichs, T., Taraborrelli, D., Cazorla, M., Fadnavis, S., Buchholz, R. R., Gaubert, B., Rojas, N. Y., Nogueira, T., Salameh, T., and Huang, M.: Tropospheric ozone precursors: global and regional distributions, trends, and variability, *Atmospheric Chemistry and Physics*, 24, 12 225–12 257, <https://doi.org/10.5194/acp-24-12225-2024>, publisher: Copernicus GmbH, 2024.

- Fadnavis, S., Elshorbany, Y., Ziemke, J., Barret, B., Rap, A., Chandran, P. R. S., Pope, R., Sagar, V., Taraborrelli, D., Le Flochmoen, E.,
490 Cuesta, J., Wespes, C., Boersma, F., Glissenaar, I., De Smedt, I., Van Roozendaal, M., Petetin, H., and Anglou, I.: Influence of nitrogen
oxides and volatile organic compounds emission changes on tropospheric ozone variability, trends and radiative effect, *EGUsphere*, pp.
1–51, <https://doi.org/10.5194/egusphere-2024-3050>, publisher: Copernicus GmbH, 2024.
- Froidevaux, L., Kinnison, D. E., Gaubert, B., Schwartz, M. J., Livesey, N. J., Read, W. G., Bardeen, C. G., Ziemke, J. R., and Fuller, R. A.:
Tropical upper tropospheric trends in ozone and carbon monoxide (2005–2020): observational and model results, *EGUsphere*, pp.
495 1–59, <https://doi.org/10.5194/egusphere-2024-525>, publisher: Copernicus GmbH, 2024.
- Fu, D., Worden, J. R., Liu, X., Kulawik, S. S., Bowman, K. W., and Natraj, V.: Characterization of ozone profiles derived from Aura TES
and OMI radiances, *Atmospheric Chemistry and Physics*, 13, 3445–3462, <https://doi.org/10.5194/acp-13-3445-2013>, 2013.
- Fu, D., Bowman, K. W., Worden, H. M., Natraj, V., Worden, J. R., Yu, S., Veefkind, P., Aben, I., Landgraf, J., Strow, L., and Han, Y.:
High-resolution tropospheric carbon monoxide profiles retrieved from CrIS and TROPOMI, *Atmospheric Measurement Techniques*, 9,
500 2567–2579, <https://doi.org/10.5194/amt-9-2567-2016>, 2016.
- Fu, D., Kulawik, S. S., Miyazaki, K., Bowman, K. W., Worden, J. R., Eldering, A., Livesey, N. J., Teixeira, J., Irion, F. W., Herman, R. L.,
Osterman, G. B., Liu, X., Levelt, P. F., Thompson, A. M., and Luo, M.: Retrievals of tropospheric ozone profiles from the synergism
of AIRS and OMI: methodology and validation, *Atmospheric Measurement Techniques*, 11, 5587–5605, [https://doi.org/10.5194/amt-11-](https://doi.org/10.5194/amt-11-5587-2018)
5587-2018, 2018.
- 505 Gaudel, A., Cooper, O. R., Ancellet, G., Barret, B., Boynard, A., Burrows, J. P., Clerbaux, C., Coheur, P.-F., Cuesta, J., Cuevas, E., Doniki,
S., Dufour, G., Ebojie, F., Foret, G., Garcia, O., Granados-Muñoz, M. J., Hannigan, J. W., Hase, F., Hassler, B., Huang, G., Hurtmans,
D., Jaffe, D., Jones, N., Kalabokas, P., Kerridge, B., Kulawik, S., Latter, B., Leblanc, T., Le Flochmoën, E., Lin, W., Liu, J., Liu, X.,
Mahieu, E., McClure-Begley, A., Neu, J. L., Osman, M., Palm, M., Petetin, H., Petropavlovskikh, I., Querel, R., Rahpoe, N., Rozanov,
A., Schultz, M. G., Schwab, J., Siddans, R., Smale, D., Steinbacher, M., Tanimoto, H., Tarasick, D. W., Thouret, V., Thompson, A. M.,
510 Trickl, T., Weatherhead, E., Wespes, C., Worden, H. M., Vigouroux, C., Xu, X., Zeng, G., and Ziemke, J.: Tropospheric Ozone Assessment
Report: Present-day distribution and trends of tropospheric ozone relevant to climate and global atmospheric chemistry model evaluation,
Elementa: Science of the Anthropocene, 6, 39, <https://doi.org/10.1525/elementa.291>, 2018.
- Gaudel, A., Bourgeois, I., Li, M., Chang, K.-L., Ziemke, J., Sauvage, B., Stauffer, R. M., Thompson, A. M., Kollonige, D. E., Smith, N.,
Hubert, D., Keppens, A., Cuesta, J., Heue, K.-P., Veefkind, P., Aikin, K., Peischl, J., Thompson, C. R., Ryerson, T. B., Frost, G. J.,
515 McDonald, B. C., and Cooper, O. R.: Tropical tropospheric ozone distribution and trends from in situ and satellite data, *Atmospheric
Chemistry and Physics*, 24, 9975–10 000, <https://doi.org/10.5194/acp-24-9975-2024>, publisher: Copernicus GmbH, 2024.
- GMAO: GEOS FP-IT data, https://gmao.gsfc.nasa.gov/GMAO_products/NRT_products.php, 2024.
- Gulev, S. K., Thorne, P. W., Ahn, J., Dentener, F. J., Domingues, C. M., Gerland, S., Gong, D., Kaufman, D. S., Nnamchi, H. C., Quaas,
J., Rivera, J. A., Sathyendranath, S., Smith, S. L., Trewin, B., von Schuckmann, K., and Vose, R. S.: Changing State of the Climate
520 System, in: *Climate Change 2021: The Physical Science Basis. Contribution of Working Group I to the Sixth Assessment Report of the
Intergovernmental Panel on Climate Change*, edited by Masson-Delmotte, V., Zhai, P., Pirani, A., Connors, S. L., Pean, C., Berger, S.,
Caud, N., Chen, Y., Goldfarb, L., Gomis, M. I., Huang, M., Leitzell, K., Lonnoy, E., Matthews, J. B. R., Maycock, T. K., Waterfield, T.,
Yelekci, O., Yu, R., and Zhou, B., pp. 287–422, Cambridge University Press, Cambridge, United Kingdom and New York, NY, USA,
doi:10.1017/9781009157896.004, 2021.
- 525 Han, Y.: CrIS Full Spectral Resolution SDR and S-NPP/JPSS-1 CrIS Performance Status, [https://www.star.nesdis.noaa.gov/jpss/documents/
meetings/2015/ITSC-XX/Yong_Han_2015ITSC-20_1p07.pdf](https://www.star.nesdis.noaa.gov/jpss/documents/meetings/2015/ITSC-XX/Yong_Han_2015ITSC-20_1p07.pdf), 2015.

- Han, Y., Revercomb, H., Crompt, M., Gu, D., Johnson, D., Mooney, D., Scott, D., Strow, L., Bingham, G., Borg, L., Chen, Y., DeSlover, D., Esplin, M., Hagan, D., Jin, X., Knuteson, R., Motteler, H., Predina, J., Suwinski, L., Taylor, J., Tobin, D., Tremblay, D., Wang, C., Wang, L., Wang, L., and Zavyalov, V.: Suomi NPP CrIS measurements, sensor data record algorithm, calibration and validation activities, and record data quality, *Journal of Geophysical Research: Atmospheres*, 118, 12,734–12,748, <https://doi.org/10.1002/2013JD020344>, *_eprint: https://onlinelibrary.wiley.com/doi/pdf/10.1002/2013JD020344*, 2013.
- HEGIFTOM: Ozonesondes: Harmonization and Evaluation of Ground-based Instruments for Free Tropospheric Ozone Measurements., <https://hegiftom.meteo.be/datasets/ozonesondes>, 2024.
- Heue, K.-P., Coldewey-Egbers, M., Delcloo, A., Lerot, C., Loyola, D., Valks, P., and van Roozendael, M.: Trends of tropical tropospheric ozone from 20 years of European satellite measurements and perspectives for the Sentinel-5 Precursor, *Atmospheric Measurement Techniques*, 9, 5037–5051, <https://doi.org/10.5194/amt-9-5037-2016>, publisher: Copernicus GmbH, 2016.
- Huang, G., Liu, X., Chance, K., Yang, K., Bhartia, P. K., Cai, Z., Allaart, M., Ancellet, G., Calpini, B., Coetzee, G. J. R., Cuevas-Agulló, E., Cupeiro, M., De Backer, H., Dubey, M. K., Fuelberg, H. E., Fujiwara, M., Godin-Beekmann, S., Hall, T. J., Johnson, B., Joseph, E., Kivi, R., Kois, B., Komala, N., König-Langlo, G., Laneve, G., Leblanc, T., Marchand, M., Minschwaner, K. R., Morris, G., Newchurch, M. J., Ogino, S.-Y., Ohkawara, N., Piters, A. J. M., Posny, F., Querel, R., Scheele, R., Schmidlin, F. J., Schnell, R. C., Schrems, O., Selkirk, H., Shiotani, M., Skrivánková, P., Stübi, R., Taha, G., Tarasick, D. W., Thompson, A. M., Thouret, V., Tully, M. B., Van Malderen, R., Vömel, H., von der Gathen, P., Witte, J. C., and Yela, M.: Validation of 10-year SAO OMI Ozone Profile (PROFOZ) product using ozonesonde observations, *Atmospheric Measurement Techniques*, 10, 2455–2475, <https://doi.org/10.5194/amt-10-2455-2017>, publisher: Copernicus GmbH, 2017.
- Iturbide-Sanchez, F., Strow, L., Tobin, D., Chen, Y., Tremblay, D., Knuteson, R. O., Johnson, D. G., Buttles, C., Suwinski, L., Thomas, B. P., Rivera, A. R., Lynch, E., Zhang, K., Wang, Z., Porter, W. D., Jin, X., Predina, J. P., Eresmaa, R. I., Collard, A., Ruston, B., Jung, J. A., Barnet, C. D., Beierle, P. J., Yan, B., Mooney, D., and Revercomb, H.: Recalibration and Assessment of the SNPP CrIS Instrument: A Successful History of Restoration After Midwave Infrared Band Anomaly, *IEEE Transactions on Geoscience and Remote Sensing*, 60, 1–21, <https://doi.org/10.1109/TGRS.2021.3112400>, conference Name: IEEE Transactions on Geoscience and Remote Sensing, 2022.
- Jiang, Y. B., Froidevaux, L., Lambert, A., Livesey, N. J., Read, W. G., Waters, J. W., Bojkov, B., Leblanc, T., McDermid, I. S., Godin-Beekmann, S., Filipiak, M. J., Harwood, R. S., Fuller, R. A., Daffer, W. H., Drouin, B. J., Cofield, R. E., Cuddy, D. T., Jarnot, R. F., Knosp, B. W., Perun, V. S., Schwartz, M. J., Snyder, W. V., Stek, P. C., Thurstans, R. P., Wagner, P. A., Allaart, M., Andersen, S. B., Bodeker, G., Calpini, B., Claude, H., Coetzee, G., Davies, J., De Backer, H., Dier, H., Fujiwara, M., Johnson, B., Kelder, H., Leme, N. P., König-Langlo, G., Kyro, E., Laneve, G., Fook, L. S., Merrill, J., Morris, G., Newchurch, M., Oltmans, S., Parrondos, M. C., Posny, F., Schmidlin, F., Skrivankova, P., Stubi, R., Tarasick, D., Thompson, A., Thouret, V., Viatte, P., Vömel, H., von Der Gathen, P., Yela, M., and Zabolocki, G.: Validation of Aura Microwave Limb Sounder Ozone by ozonesonde and lidar measurements, *Journal of Geophysical Research: Atmospheres*, 112, <https://doi.org/10.1029/2007JD008776>, *_eprint: https://onlinelibrary.wiley.com/doi/pdf/10.1029/2007JD008776*, 2007.
- Jones, D. B. A., Bowman, K. W., Palmer, P. I., Worden, J. R., Jacob, D. J., Hoffman, R. N., Bey, I., and Yantosca, R. M.: Potential of observations from the Tropospheric Emission Spectrometer to constrain continental sources of carbon monoxide, *Journal of Geophysical Research: Atmospheres*, 108, <https://doi.org/10.1029/2003JD003702>, *_eprint: https://onlinelibrary.wiley.com/doi/pdf/10.1029/2003JD003702*, 2003.
- Komhyr, W. D.: Electrochemical concentration cells for gas analysis, *Annales Geophysicae*, pp. 203–210, 1969.
- Komhyr, W. D. and Harris, T. B.: Development of an ECC Ozonesonde, Tech. Rep. ERL 200-APCL 18, 1971.

Levelt, P., van den Oord, G., Dobber, M., Malkki, A., Visser, H., Vries, J. d., Stammes, P., Lundell, J., and Saari, H.: The ozone monitoring instrument, *IEEE Transactions on Geoscience and Remote Sensing*, 44, 1093–1101, <https://doi.org/10.1109/TGRS.2006.872333>, conference Name: IEEE Transactions on Geoscience and Remote Sensing, 2006.

Levelt, P. F., Joiner, J., Tamminen, J., Veefkind, J. P., Bhartia, P. K., Stein Zweers, D. C., Duncan, B. N., Streets, D. G., Eskes, H., van der A, R., McLinden, C., Fioletov, V., Carn, S., de Laat, J., DeLand, M., Marchenko, S., McPeters, R., Ziemke, J., Fu, D., Liu, X., Pickering, K., Apituley, A., González Abad, G., Arola, A., Boersma, F., Chan Miller, C., Chance, K., de Graaf, M., Hakkarainen, J., Hassinen, S., Ialongo, I., Kleipool, Q., Krotkov, N., Li, C., Lamsal, L., Newman, P., Nowlan, C., Suleiman, R., Tilstra, L. G., Torres, O., Wang, H., and Wargan, K.: The Ozone Monitoring Instrument: overview of 14 years in space, *Atmospheric Chemistry and Physics*, 18, 5699–5745, <https://doi.org/10.5194/acp-18-5699-2018>, publisher: Copernicus GmbH, 2018.

Leventidou, E., Weber, M., Eichmann, K.-U., Burrows, J. P., Heue, K.-P., Thompson, A. M., and Johnson, B. J.: Harmonisation and trends of 20-year tropical tropospheric ozone data, *Atmospheric Chemistry and Physics*, 18, 9189–9205, <https://doi.org/10.5194/acp-18-9189-2018>, publisher: Copernicus GmbH, 2018.

Liu, X., Bhartia, P. K., Chance, K., Froidevaux, L., Spurr, R. J. D., and Kurosu, T. P.: Validation of Ozone Monitoring Instrument (OMI) ozone profiles and stratospheric ozone columns with Microwave Limb Sounder (MLS) measurements, *Atmospheric Chemistry and Physics*, 10, 2539–2549, <https://doi.org/10.5194/acp-10-2539-2010>, publisher: Copernicus GmbH, 2010a.

Liu, X., Bhartia, P. K., Chance, K., Spurr, R. J. D., and Kurosu, T. P.: Ozone profile retrievals from the Ozone Monitoring Instrument, *Atmospheric Chemistry and Physics*, 10, 2521–2537, <https://doi.org/10.5194/acp-10-2521-2010>, publisher: Copernicus GmbH, 2010b.

Livesey, N. J., Read, W. G., Wagner, P. A., Froidevaux, L., Santee, M. L., Schwartz, M. J., Lambert, A., Millan Valle, L. F., Pumphrey, H. C., Manney, G. L., Fuller, R. A., Jarnot, R. F., Knosp, B. W., and Lay, R. R.: Version 5.0x Level 2 and 3 data quality and description document, Tech. Rep. JPL D-105336 Rev. B, Jet Propulsion Laboratory, California Institute of Technology, https://mls.jpl.nasa.gov/data/v5-0_data_quality_document.pdf, 2022.

Lucchesi, R.: File Specification for GEOS-5 FP-IT (Forward Processing for Instrument Teams), Tech. Rep. GMAO Office Note No. 2 (Version 1.3), <https://gmao.gsfc.nasa.gov/pubs/docs/Lucchesi865.pdf>, 2015.

Malina, E., Bowman, K. W., Kantchev, V., Kuai, L., Kurosu, T. P., Miyazaki, K., Natraj, V., Osterman, G. B., Oyafuso, F., and Thill, M. D.: Joint spectral retrievals of ozone with Suomi NPP CrIS augmented by S5P/TROPOMI, *Atmospheric Measurement Techniques*, 17, 5341–5371, <https://doi.org/10.5194/amt-17-5341-2024>, publisher: Copernicus GmbH, 2024.

Manney, G. L., Hegglin, M. I., Daffer, W. H., Schwartz, M. J., Santee, M. L., and Pawson, S.: Climatology of Upper Tropospheric–Lower Stratospheric (UTLS) Jets and Tropopause in MERRA, <https://doi.org/10.1175/JCLI-D-13-00243.1>, section: Journal of Climate, 2014.

Manney, G. L., Hegglin, M. I., Lawrence, Z. D., Wargan, K., Millán, L. F., Schwartz, M. J., Santee, M. L., Lambert, A., Pawson, S., Knosp, B. W., Fuller, R. A., and Daffer, W. H.: Reanalysis comparisons of upper tropospheric–lower stratospheric jets and multiple tropopause, *Atmospheric Chemistry and Physics*, 17, 11 541–11 566, <https://doi.org/10.5194/acp-17-11541-2017>, publisher: Copernicus GmbH, 2017.

Miles, G. M., Siddans, R., Kerridge, B. J., Latter, B. G., and Richards, N. a. D.: Tropospheric ozone and ozone profiles retrieved from GOME-2 and their validation, *Atmospheric Measurement Techniques*, 8, 385–398, <https://doi.org/10.5194/amt-8-385-2015>, publisher: Copernicus GmbH, 2015.

Miyazaki, K., Eskes, H., Sudo, K., Boersma, K. F., Bowman, K., and Kanaya, Y.: Decadal changes in global surface NO_x emissions from multi-constituent satellite data assimilation, *Atmospheric Chemistry and Physics*, 17, 807–837, <https://doi.org/10.5194/acp-17-807-2017>, publisher: Copernicus GmbH, 2017.

- Miyazaki, K., Sekiya, T., Fu, D., Bowman, K. W., Kulawik, S. S., Sudo, K., Walker, T., Kanaya, Y., Takigawa, M., Ogochi, K., Eskes, H., Boersma, K. F., Thompson, A. M., Gaubert, B., Barre, J., and Emmons, L. K.: Balance of Emission and Dynamical Controls on Ozone During the Korea-United States Air Quality Campaign From Multiconstituent Satellite Data Assimilation, *Journal of Geophysical Research: Atmospheres*, 124, 387–413, <https://doi.org/10.1029/2018JD028912>, _eprint: <https://onlinelibrary.wiley.com/doi/pdf/10.1029/2018JD028912>, 2019.
- Miyazaki, K., Bowman, K., Sekiya, T., Eskes, H., Boersma, F., Worden, H., Livesey, N., Payne, V. H., Sudo, K., Kanaya, Y., Takigawa, M., and Ogochi, K.: Updated tropospheric chemistry reanalysis and emission estimates, TCR-2, for 2005–2018, *Earth System Science Data*, 12, 2223–2259, <https://doi.org/10.5194/essd-12-2223-2020>, publisher: Copernicus GmbH, 2020a.
- Miyazaki, K., Bowman, K. W., Yumimoto, K., Walker, T., and Sudo, K.: Evaluation of a multi-model, multi-constituent assimilation framework for tropospheric chemical reanalysis, *Atmospheric Chemistry and Physics*, 20, 931–967, <https://doi.org/10.5194/acp-20-931-2020>, publisher: Copernicus GmbH, 2020b.
- Miyazaki, K., Bowman, K., Sekiya, T., Takigawa, M., Neu, J. L., Sudo, K., Osterman, G., and Eskes, H.: Global tropospheric ozone responses to reduced NO_x emissions linked to the COVID-19 worldwide lockdowns, *Science Advances*, 7, eabf7460, <https://doi.org/10.1126/sciadv.abf7460>, publisher: American Association for the Advancement of Science, 2021.
- Molod, A., Takacs, L., Suarez, M., Bacmeister, J., Song, I.-S., and Eichmann, A.: The GEOS-5 Atmospheric General Circulation Model: Mean Climate and Development from MERRA to Fortuna, Tech. Rep. NASA/TM–2012-104606/Vol 28, NASA Goddard Space Flight Center, Greenbelt, Maryland, 2012.
- NASA: TROPESS, <https://tes.jpl.nasa.gov/tropess/>, <https://tes.jpl.nasa.gov/tropess/>, 2024.
- Nassar, R., Logan, J. A., Worden, H. M., Megretskaya, I. A., Bowman, K. W., Osterman, G. B., Thompson, A. M., Tarasick, D. W., Austin, S., Claude, H., Dubey, M. K., Hocking, W. K., Johnson, B. J., Joseph, E., Merrill, J., Morris, G. A., Newchurch, M., Oltmans, S. J., Posny, F., Schmidlin, F. J., Vömel, H., Whiteman, D. N., and Witte, J. C.: Validation of Tropospheric Emission Spectrometer (TES) nadir ozone profiles using ozonesonde measurements, *Journal of Geophysical Research: Atmospheres*, 113, <https://doi.org/10.1029/2007JD008819>, _eprint: <https://onlinelibrary.wiley.com/doi/pdf/10.1029/2007JD008819>, 2008.
- NOAA: CrIS on SNPP switch to side 1 on July 12, 2021, <https://www.ospo.noaa.gov/data/messages/2021/MSG188150401.html>, 2021.
- Osterman, G. B., Kulawik, S. S., Worden, H. M., Richards, N. a. D., Fisher, B. M., Eldering, A., Shephard, M. W., Froidevaux, L., Labow, G., Luo, M., Herman, R. L., Bowman, K. W., and Thompson, A. M.: Validation of Tropospheric Emission Spectrometer (TES) measurements of the total, stratospheric, and tropospheric column abundance of ozone, *Journal of Geophysical Research: Atmospheres*, 113, <https://doi.org/10.1029/2007JD008801>, _eprint: <https://onlinelibrary.wiley.com/doi/pdf/10.1029/2007JD008801>, 2008.
- Parrington, M., Jones, D. B. A., Bowman, K. W., Thompson, A. M., Tarasick, D. W., Merrill, J., Oltmans, S. J., Leblanc, T., Witte, J. C., and Millet, D. B.: Impact of the assimilation of ozone from the Tropospheric Emission Spectrometer on surface ozone across North America, *Geophysical Research Letters*, 36, <https://doi.org/10.1029/2008GL036935>, _eprint: <https://onlinelibrary.wiley.com/doi/pdf/10.1029/2008GL036935>, 2009.
- Pope, R. J., Kerridge, B. J., Siddans, R., Latter, B. G., Chipperfield, M. P., Feng, W., Pimlott, M. A., Dhomse, S. S., Retscher, C., and Rigby, R.: Investigation of spatial and temporal variability in lower tropospheric ozone from RAL Space UV–Vis satellite products, *Atmospheric Chemistry and Physics*, 23, 14 933–14 947, <https://doi.org/10.5194/acp-23-14933-2023>, publisher: Copernicus GmbH, 2023.
- Pope, R. J., O'Connor, F. M., Dalvi, M., Kerridge, B. J., Siddans, R., Latter, B. G., Barret, B., Le Flochmoen, E., Boynard, A., Chipperfield, M. P., Feng, W., Pimlott, M. A., Dhomse, S. S., Retscher, C., Wespes, C., and Rigby, R.: Investigation of the impact of satel-

- lite vertical sensitivity on long-term retrieved lower-tropospheric ozone trends, *Atmospheric Chemistry and Physics*, 24, 9177–9195, <https://doi.org/10.5194/acp-24-9177-2024>, publisher: Copernicus GmbH, 2024.
- 640 Revercomb, H. and Strow, L.: Suomi NPP CrIS Level 1B Full Spectral Resolution V2, <https://doi.org/10.5067/9NPOTPIPLMAW>, 2018.
- Schenkeveld, V. M. E., Jaross, G., Marchenko, S., Haffner, D., Kleipool, Q. L., Rozemeijer, N. C., Veefkind, J. P., and Levelt, P. F.: In-flight performance of the Ozone Monitoring Instrument, *Atmospheric Measurement Techniques*, 10, 1957–1986, <https://doi.org/10.5194/amt-10-1957-2017>, publisher: Copernicus GmbH, 2017.
- Smith, N. and Barnett, C. D.: CLIMCAPS observing capability for temperature, moisture, and trace gases from AIRS/AMSU and CrIS/ATMS, *Atmospheric Measurement Techniques*, 13, 4437–4459, <https://doi.org/10.5194/amt-13-4437-2020>, publisher: Copernicus GmbH, 2020.
- 645 Steinbrecht, W., Schwarz, R., and Claude, H.: New Pump Correction for the Brewer–Mast Ozone Sonde: Determination from Experiment and Instrument Intercomparisons, [https://doi.org/https://doi.org/10.1175/1520-0426\(1998\)015<0144:NPCFTB>2.0.CO;2](https://doi.org/https://doi.org/10.1175/1520-0426(1998)015<0144:NPCFTB>2.0.CO;2), section: Journal of Atmospheric and Oceanic Technology, 1998.
- Stephens, G. L., Vane, D. G., Boain, R. J., Mace, G. G., Sassen, K., Wang, Z., Illingworth, A. J., O’connor, E. J., Rossow, W. B.,
- 650 Durden, S. L., Miller, S. D., Austin, R. T., Benedetti, A., and Mitrescu, C.: THE CLOUDSAT MISSION AND THE A-TRAIN, <https://doi.org/10.1175/BAMS-83-12-1771>, section: Bulletin of the American Meteorological Society, 2002.
- Strow, L. L., Motteler, H., Tobin, D., Revercomb, H., Hannon, S., Buijs, H., Predina, J., Suwinski, L., and Glumb, R.: Spectral calibration and validation of the Cross-track Infrared Sounder on the Suomi NPP satellite, *Journal of Geophysical Research: Atmospheres*, 118, 12,486–12,496, <https://doi.org/10.1002/2013JD020480>, _eprint: <https://onlinelibrary.wiley.com/doi/pdf/10.1002/2013JD020480>, 2013.
- 655 Susskind, J., Barnett, C., and Blaisdell, J.: Retrieval of atmospheric and surface parameters from AIRS/AMSU/HSB data in the presence of clouds, *IEEE Transactions on Geoscience and Remote Sensing*, 41, 390–409, <https://doi.org/10.1109/TGRS.2002.808236>, conference Name: IEEE Transactions on Geoscience and Remote Sensing, 2003.
- Susskind, J., Blaisdell, J. M., and Iredell, L.: Improved methodology for surface and atmospheric soundings, error estimates, and quality control procedures: the atmospheric infrared sounder science team version-6 retrieval algorithm, *Journal of Applied Remote Sensing*, 8, 084 994, <https://doi.org/10.1117/1.JRS.8.084994>, publisher: SPIE, 2014.
- 660 Tarasick, D., Galbally, I. E., Cooper, O. R., Schultz, M. G., Ancellet, G., Leblanc, T., Wallington, T. J., Ziemke, J., Liu, X., Steinbacher, M., Staehelin, J., Vigouroux, C., Hannigan, J. W., García, O., Foret, G., Zanis, P., Weatherhead, E., Petropavlovskikh, I., Worden, H., Osman, M., Liu, J., Chang, K.-L., Gaudel, A., Lin, M., Granados-Muñoz, M., Thompson, A. M., Oltmans, S. J., Cuesta, J., Dufour, G., Thouret, V., Hassler, B., Trickl, T., and Neu, J. L.: Tropospheric Ozone Assessment Report: Tropospheric ozone from 1877 to 2016, observed levels, trends and uncertainties, *Elementa: Science of the Anthropocene*, 7, 39, <https://doi.org/10.1525/elementa.376>, 2019.
- Tarasick, D. W., Smit, H. G. J., Thompson, A. M., Morris, G. A., Witte, J. C., Davies, J., Nakano, T., Van Malderen, R., Stauffer, R. M., Johnson, B. J., Stübi, R., Oltmans, S. J., and Vömel, H.: Improving ECC Ozonesonde Data Quality: Assessment of Current Methods and Outstanding Issues, *Earth and Space Science*, 8, e2019EA000 914, <https://doi.org/10.1029/2019EA000914>, _eprint: <https://onlinelibrary.wiley.com/doi/pdf/10.1029/2019EA000914>, 2021.
- 670 Tobin, D., Revercomb, H., Knuteson, R., Taylor, J., Best, F., Borg, L., DeSlover, D., Martin, G., Buijs, H., Esplin, M., Glumb, R., Han, Y., Mooney, D., Predina, J., Strow, L., Suwinski, L., and Wang, L.: Suomi-NPP CrIS radiometric calibration uncertainty, *Journal of Geophysical Research: Atmospheres*, 118, 10,589–10,600, <https://doi.org/10.1002/jgrd.50809>, _eprint: <https://onlinelibrary.wiley.com/doi/pdf/10.1002/jgrd.50809>, 2013.
- Van Malderen, R., Thompson, A. M., Kollonige, D. E., Stauffer, R. M., Smit, H. G. J., Maillard Barras, E., Vigouroux, C., Petropavlovskikh,
- 675 I., Leblanc, T., Thouret, V., Wolff, P., Effertz, P., Tarasick, D. W., Poyraz, D., Ancellet, G., De Backer, M.-R., Evan, S., Flood, V.,

- Frey, M. M., Hannigan, J. W., Hernandez, J. L., Iarlori, M., Johnson, B. J., Jones, N., Kivi, R., Mahieu, E., McConville, G., Müller, K., Nagahama, T., Notholt, J., Piters, A., Prats, N., Querel, R., Smale, D., Steinbrecht, W., Strong, K., and Sussmann, R.: Global Ground-based Tropospheric Ozone Measurements: Reference Data and Individual Site Trends (2000–2022) from the TOAR-II/HEGIFTOM Project, EGU sphere, pp. 1–53, <https://doi.org/10.5194/egusphere-2024-3736>, publisher: Copernicus GmbH, 2025.
- 680 Verstraeten, W. W., Boersma, K. F., Zörner, J., Allaart, M. a. F., Bowman, K. W., and Worden, J. R.: Validation of six years of TES tropospheric ozone retrievals with ozonesonde measurements: implications for spatial patterns and temporal stability in the bias, *Atmospheric Measurement Techniques*, 6, 1413–1423, <https://doi.org/10.5194/amt-6-1413-2013>, publisher: Copernicus GmbH, 2013.
- Wang, L., Tremblay, D. A., Han, Y., Esplin, M., Hagan, D. E., Predina, J., Suwinski, L., Jin, X., and Chen, Y.: Geolocation assessment for CrIS sensor data records, *Journal of Geophysical Research: Atmospheres*, 118, 12,690–12,704, <https://doi.org/10.1002/2013JD020376>,
685 _eprint: <https://onlinelibrary.wiley.com/doi/pdf/10.1002/2013JD020376>, 2013.
- Waters, J., Froidevaux, L., Harwood, R., Jarnot, R., Pickett, H., Read, W., Siegel, P., Cofield, R., Filipiak, M., Flower, D., Holden, J., Lau, G., Livesey, N., Manney, G., Pumphrey, H., Santee, M., Wu, D., Cuddy, D., Lay, R., Loo, M., Perun, V., Schwartz, M., Stek, P., Thurstans, R., Boyles, M., Chandra, K., Chavez, M., Chen, G.-S., Chudasama, B., Dodge, R., Fuller, R., Girard, M., Jiang, J., Jiang, Y., Knosp, B., LaBelle, R., Lam, J., Lee, K., Miller, D., Oswald, J., Patel, N., Pukala, D., Quintero, O., Scaff, D., Van Snyder, W., Tope, M., Wagner, P.,
690 and Walch, M.: The Earth observing system microwave limb sounder (EOS MLS) on the aura Satellite, *IEEE Transactions on Geoscience and Remote Sensing*, 44, 1075–1092, <https://doi.org/10.1109/TGRS.2006.873771>, conference Name: IEEE Transactions on Geoscience and Remote Sensing, 2006.
- Wei, J. C., Pan, L. L., Maddy, E., Pittman, J. V., Divarkarla, M., Xiong, X., and Barnet, C.: Ozone Profile Retrieval from an Advanced Infrared Sounder: Experiments with Tropopause-Based Climatology and Optimal Estimation Approach,
695 <https://doi.org/10.1175/2010JTECHA1384.1>, section: Journal of Atmospheric and Oceanic Technology, 2010.
- Werner, F., Livesey, N. J., Millán, L. F., Read, W. G., Schwartz, M. J., Wagner, P. A., Daffer, W. H., Lambert, A., Tolstoff, S. N., and Santee, M. L.: Applying machine learning to improve the near-real-time products of the Aura Microwave Limb Sounder, *Atmospheric Measurement Techniques*, 16, 2733–2751, <https://doi.org/10.5194/amt-16-2733-2023>, publisher: Copernicus GmbH, 2023.
- WMO: Meteorology - A three-dimensional science: Second session of the commission for aerology, *WMO Bulletin*, 6, 134–138, 1957.
- 700 WMO: Ozonesonde Measurement Principles and Best Operational Practices: ASOPOS 2.0 (Assessment of Standard Operating Procedures for Ozonesondes), GAW Report No. 268, World Meteorological Organization (WMO), Geneva, Switzerland, <https://library.wmo.int/idurl/4/57720>, 2021.
- WMO/GAW: World Meteorological Organization-Global Atmosphere Watch Program (WMO-GAW)/World Ozone and Ultraviolet Radiation Data Centre (WOUDC), <https://doi.org/doi:10.14287/10000001>, a list of all contributors is available on the website, 2024.
- 705 Worden, H. M., Logan, J. A., Worden, J. R., Beer, R., Bowman, K., Clough, S. A., Eldering, A., Fisher, B. M., Gunson, M. R., Herman, R. L., Kulawik, S. S., Lampel, M. C., Luo, M., Megretskaia, I. A., Osterman, G. B., and Shephard, M. W.: Comparisons of Tropospheric Emission Spectrometer (TES) ozone profiles to ozonesondes: Methods and initial results, *Journal of Geophysical Research: Atmospheres*, 112, <https://doi.org/10.1029/2006JD007258>, _eprint: <https://onlinelibrary.wiley.com/doi/pdf/10.1029/2006JD007258>, 2007.
- Wu, W., Liu, X., Lei, L., Xiong, X., Yang, Q., Yue, Q., Zhou, D. K., and Larar, A. M.: Single field-of-view sounder atmospheric product retrieval algorithm: establishing radiometric consistency for hyper-spectral sounder retrievals, *Atmospheric Measurement Techniques*, 16,
710 4807–4832, <https://doi.org/10.5194/amt-16-4807-2023>, publisher: Copernicus GmbH, 2023.
- Ziemke, J. R., Oman, L. D., Strode, S. A., Douglass, A. R., Olsen, M. A., McPeters, R. D., Bhartia, P. K., Froidevaux, L., Labow, G. J., Witte, J. C., Thompson, A. M., Haffner, D. P., Kramarova, N. A., Frith, S. M., Huang, L.-K., Jaross, G. R., Seftor, C. J., Deland, M. T., and Taylor,

715 S. L.: Trends in global tropospheric ozone inferred from a composite record of TOMS/OMI/MLS/OMPS satellite measurements and the
MERRA-2 GMI simulation, *Atmospheric Chemistry and Physics*, 19, 3257–3269, <https://doi.org/10.5194/acp-19-3257-2019>, publisher:
Copernicus GmbH, 2019.